ERJ Express. Published on December 21, 2018 as doi: 10.1183/13993003.01562-2018

EUROPEAN RESPIRATORY *journal*

FLAGSHIP SCIENTIFIC JOURNAL OF ERS

Early View

Original article

Role of anlotinib-induced CCL2 decrease in anti-angiogenesis and response prediction for non-small cell lung cancer therapy

Jun Lu, Hua Zhong, Tianqing Chu, Xueyan Zhang, Rong Li, Jiayuan Sun, Runbo Zhong, Yuqin Yang, Mohammad Shah Alam, Yuqing Lou, Jianlin Xu, Yanwei Zhang, Jun Wu, Xiaowei Li, Xiaodong Zhao, Kai Li, Liming Lu, Baohui Han

Please cite this article as: Lu J, Zhong H, Chu T, *et al*. Role of anlotinib-induced CCL2 decrease in anti-angiogenesis and response prediction for non-small cell lung cancer therapy. *Eur Respir J* 2018; in press (https://doi.org/10.1183/13993003.01562-2018).

✧ **Original Article**

Role of anlotinib-induced CCL2 decrease in anti-angiogenesis and response prediction for non-small cell lung cancer therapy

Jun Lu[1,2,7], Hua Zhong[1,7], Tianqing Chu[1], Xueyan Zhang[1], Rong Li[1], Jiayuan Sun[1], Runbo Zhong[1], Yuqin Yang[2], Mohammad Shah Alam[3], Yuqing Lou[1], Jianlin Xu[1], Yanwei Zhang[1], Jun Wu[4], Xiaowei Li[3], Xiaodong Zhao*[,5], Kai Li*[,6], Liming Lu*[,2], Baohui Han*[,1]

[1]Department of Pulmonary, Shanghai Chest Hospital, Shanghai Jiao Tong University, Shanghai, China

[2]Central laboratory, Shanghai Chest Hospital, Shanghai Jiao Tong University, Shanghai, China

[3]Bio-ID Center, School of Biomedical Engineering, Shanghai Jiao Tong University, Shanghai, China

[4]School of Life Science, East China Normal University, Shanghai, China

[5]Shanghai Center for Systems Biomedicine, Shanghai Jiao Tong University, Shanghai, China

[6]Department of Thoracic Oncology, National Clinical Research Center for Cancer, Tianjin Medical University Cancer Institute and Hospital, Tianjin, China

[7]These authors contributed equally: Jun Lu and Hua Zhong

***Corresponding authors:**
Baohui Han, MD, Ph D, Department of Pulmonary Medicine, Shanghai Chest Hospital, Shanghai Jiao Tong University, Shanghai 200030, China. E-mail: xkyyhan@gmail.com

Liming Lu, Ph D, Central Laboratory, Shanghai Chest Hospital, Shanghai Jiaotong University, Shanghai 200030,China. E-mail: lulunew2003@163.com

Kai Li, MD, Ph D, Department of Thoracic Oncology, National Clinical Research Center for Cancer, Tianjin Medical University Cancer Institute and Hospital, Tianjin, 300060, China. E-mail: likai_fnk@163.com

Xiaodong Zhao, Ph D, Shanghai Center for Systems Biomedicine, Shanghai Jiao Tong University, Shanghai, 200240, China. E-mail: xiaodongzhao@sjtu.edu.cn

Competing Interests Statement

The authors declare no potential conflicts of interest.

ABSTRACT

Background: Anlotinib has been demonstrated in clinical trials to be effective in prolonging the progression-free survival (PFS) and overall survival (OS) of refractory advanced non-small cell lung cancer (NSCLC) patients. However, the underlying molecular mechanisms and predictive biomarkers of anlotinib are still unclear.

Methods: A retrospective analysis of anlotinib administered to 294 NSCLC patients was performed to screen for underlying biomarkers of anlotinib-responsive patients. Transcriptome and functional assays were performed to understand the anti-tumour molecular mechanisms of anlotinib. Changes in serum CCL2 levels were analysed to examine the correlation of the anlotinib response between responders and non-responders.

Results: Anlotinib therapy was beneficial for prolonging OS in NSCLC patients harbouring positive driver gene mutations, especially patients harbouring the $EGFR^{T790M}$ mutation. Moreover, anlotinib inhibited angiogenesis in an NCI-H1975-derived xenograft model via inhibiting CCL2. Finally, anlotinib-induced serum CCL2 level decreases were associated with the benefits of PFS and OS in refractory advanced NSCLC patients.

Conclusions: Our study reports a novel anti-angiogenesis mechanism of anlotinib via inhibiting CCL2 in an NCI-H1975-derived xenograft model and suggests that changes in serum CCL2 levels may be used to monitor and predict clinical outcomes in anlotinib-administered refractory advanced NSCLC patients using third-line therapy

or beyond.

Key words

Anlotinib; CCL2; Anti-angiogenesis; Biomarker; Non-small cell lung cancer

Tweetable abstract @ERSpublications

The underlying molecular mechanisms and predictive biomarkers of anlotinib benefit NSCLC patients are still unclear. In this study, anlotinib-induced CCL2 decrease contributes to a novel insight for its anti-angiogenesis mechanism and responsive prediction.

INTRODUCTION

Lung cancer is the leading cause of cancer-related death worldwide. The incidence of non-small cell lung cancer (NSCLC) is reported to be 39.05 per ten thousand people, accounting for approximately 85% of all lung cancer patients.[1] Approximately 75% of patients have advanced NSCLC that is unresectable at first diagnosis and has a 5-year survival rate of less than 15%.[2, 3] Histologically, NSCLC consists mainly of squamous-cell carcinoma (LUSC) and adenocarcinoma (LUAD).[4] First-line and second-line therapies for advanced NSCLC include the inhibition of driver genes and systemic chemotherapy. For third-line therapy, there is no consolidated regimen.[5] Systemic chemotherapy for NSCLC includes conventional chemotherapeutic agents, inhibitors of angiogenesis, and inhibitors of metastasis.[6] Although advanced NSCLC patients have obtained great benefits from first-line and second-line therapies, drugs that potently prolong progression-free survival (PFS) and overall survival (OS) at third-line or over third-line therapy are still limited. Multi-targeted drugs could introduce a new opportunity for prolonging PFS and OS in refractory advanced NSCLC patients who are receiving third-line or beyond third-line therapies.[7-10]

Anlotinib is a multi-targeted receptor tyrosine kinase inhibitor (TKI) with demonstrated anti-tumour effects in various cancers.[8-12] Previous studies have indicated that anlotinib inhibits tumour growth by inhibiting signalling pathways involving angiogenesis and cell proliferation.[8, 13, 14] Recombinant enzyme assays *in vitro* have indicated that anlotinib selectively inhibits VEGFR (1, 2 and 3), PDGFR

(α and β), and FGFR (1, 2, 3 and 4), among others. Furthermore, anlotinib suppresses tumour cell growth via the inhibition of c-Kit, Ret, Aurora-B, c-FMS and DDR1.[15-17]

Recent clinical trials have indicated that anlotinib therapy prolongs PFS and OS in refractory advanced NSCLC subjected to third-line or beyond third-line therapy.[7, 9, 10] The underlying mechanism might be attributed to anlotinib-induced block of angiogenesis. However, the molecular mechanisms of the angiogenesis blocking is yet to be fully characterized. Furthermore, identifying a biomarker that can be used to monitor and predict the clinical response of advanced NSCLC patients to anlotinib is an urgent problem to be solved to improve clinical outcomes. Therefore, in the present study, we sought to explore the underlying anti-angiogenesis mechanism of anlotinib and identify possible biomarkers for monitoring and predicting the clinical outcomes of anlotinib therapy in advanced NSCLC patients receiving third-line or beyond third-line therapies.

METHODS

Patients and samples. The clinical trials and sample preparations were performed according to our previous studies.[7, 9] The trial (ALTER-0303) is registered at ClinicalTrials.gov under No. NCT02388919.

Anlotinib response stratification by subgroups. According to the histopathologic classification, all NSCLC patients were classified into LUSC or LUAD. Analysis of PFS and OS was performed based on the histopathologic classification of all

registered anlotinib-administered NSCLC patients. Classification of the positive and negative driver gene mutation (EGFR, ROS1, or ALK) was used to evaluate the response to anlotinib in LUAD patients. Furthermore, the subtypes of positive driver gene mutations were also assessed to analyse correlations with PFS and OS. Finally, the number of metastases (stratified as > 3 metastases and ≤ 3 metastases) in registered LUAD patients at the initial assessment was used to evaluate the response to anlotinib in LUAD patients.

Cell experiments. Cell culture procedures were performed according to our previous studies.[18, 19] For detailed methods on the cell viability analysis, flow cytometric analysis, cell invasion analysis, the wound-healing scratch assay and the cell immunofluorescence assay, refer to the supplementary materials.

RNA-seq. RNA-seq and bioinformatics analysis assays were performed according to our previous studies.[18, 19] Detailed information is provided in the supplementary materials. The raw data for this study are available in the EMBL database under accession number E-MTAB-5997: http://www.ebi.ac.uk/arrayexpress/.

Animal experiments. Experiments using Balb/c nude mice (SLAC Laboratory Animal, Shanghai, China) were performed according to national guidelines for welfare. Procedures for the NCI-H1975-derived xenograft model induction, grouping, drug administration, tumour volume measurements and sample collection are described in the supplementary materials.

Quantitative analysis. Histology analysis (including H&E staining and

immunofluorescent histochemistry analysis), mRNA expression analysis and ELISA analysis were performed as conventional procedures. Detailed information was provided in the supplementary materials.

Anlotinib responder analysis prediction. In this section, we aimed to understand whether the changes in serum CCL2 levels could be used to predict the clinical response of NSCLC patients treated with anlotinib. Totally 437 NSCLC patients enrolled in ALTER-0303 study, and 294 patients received anlotinib therapy. Of the 294 patients, there are 14 anlotinib responders (PFS > 80 days) with qualified blood samples at the time-points of baseline (BL), best response (BR), and progressive disease (PD), simultaneously. For comparing the differences between responders and non-responders, we picked out randomly 14 anlotinib non-responders (PFS $\leq$ 80 days) with qualified blood samples at the time-points of BL and PD. The driver gene mutation status of NSCLC patients at their first biopsy was shown in Supplementary Table 1. Serum was isolated from blood according to standard methods. CCL2 levels were detected via ELISA as previously described. CCL2 levels in NSCLC patients were compared at different time-points. Changes in CCL2 levels after anlotinib treatment were calculated based on CCL2 levels at different time-points. Anlotinib responder analysis prediction was performed based on changes in CCL2 levels.

Statistical analyses. PFS and OS were summarized as median values and two-sided 95% confidence interval and were analysed using the Kaplan-Meier method. The Mantel-Cox test was used to perform the Kaplan-Meier survival analysis in GraphPad Prism 5. All *in vitro* experiments, excluding RNA-seq, were carried out at least three

biological replicates. The values represent the mean ± SD. The data were examined using the two-tailed Student's *t*-test, log-rank test, or one-way ANOVA with posthoc Bonferroni correction. Differences were considered significant at $*P< 0.05$, $**P< 0.01$ and $***P< 0.001$.

RESULTS

LUAD patients harbouring positive driver gene mutations have a better OS after anlotinib therapy

All NSCLC patients (n = 294) received anlotinib therapy for two consecutive weeks and then discontinued for one week (Fig. 1a) until progression of disease (PD) was observed. To examine the anlotinib response of NSCLC patients, we divided the patients into LUSC (n = 54) and LUAD (n = 240) according to the histopathologic classification. Kaplan-Meier analysis suggested that there was no difference in the PFS and OS curves between LUSC and LUAD after anlotinib therapy (Supplementary Fig. 1a). Among the registered patients, LUAD accounted for the majority of all NSCLC patients. Therefore, we performed a subgroup analysis of the LUAD patients. Compared with the OS of the driver gene-negative patients (n = 147), that of the driver gene-positive patients (n = 93) was significantly longer after anlotinib therapy. However, there was no significant difference when the PFS analysis was performed (Fig. 1b, c). Subsequently, Kaplan-Meier analysis was performed to examine the correlations between mutation types of the driver gene and PFS or OS. The patients harbouring the ROS1 or $EGFR^{T790M}$ mutation had a better response to

anlotinib than those with other types of driver gene mutation (Fig. 1d, e). Further analysis suggested that the OS of patients harbouring the $EGFR^{T790M}$ mutation was significantly longer than those with other driver gene types, although differences in PFS remained in no significant (Fig. 1f, g). Furthermore, the NSCLC patients harbouring more than 3 metastases had a shorter PFS and OS than the NSCLC patients harbouring fewer than or equal to 3 metastases (Supplementary Fig. 1b). Interestingly, we found that some LUAD patients without a driver gene mutation also had a good response to anlotinib therapy (Supplementary Fig. 1c-e), suggesting potential alternative biomarkers for distinguishing anlotinib responders from non-responders.

Anlotinib induces NCI-H1975 cell cytotoxicity *in vitro* and *in vivo*

Understanding the underlying molecular mechanisms could be a prerequisite to identify valuable biomarkers for anlotinib responders. Here, we found that NCI-H1975 cells were the obviously sensitive to anlotinib *in vitro*, as demonstrated by cell apoptosis induction, cell invasion inhibition, cell cycle arrest, and cell migration inhibition (Supplementary Fig. 2a-i). These results suggested multiple cytotoxic effects of anlotinib upon NCI-H1975 cells. To examine whether anlotinib could inhibit tumour growth *in vivo*, we administered anlotinib in NCI-H1975-derived xenograft models. The timeline of the *in vivo* experiment was shown in Fig. 2a. After one cycle of anlotinib treatment, tumour growth was significantly inhibited, and the survival time was markedly enhanced, with acceptable toxicity at both dosages (Fig. 2b, c, Supplementary Fig. 2j-l). Extensive tissue necrosis, as evaluated by H&E

staining, was found in anlotinib-treated NCI-H1975-derived xenografts models, and the tumour cavity, as evaluated by CT, revealed refractory advanced NSCLC patients after anlotinib therapy (Fig. 2d, Supplementary Fig. 1c, d), indicating that anti-angiogenesis could play an important role in anlotinib-induced tumour inhibition.

Transcriptome analysis indicates that anlotinib-induced CCL2 blockade is involved in anlotinib-induced angiogenesis block

Based on the observations of cytotoxicity and tissue necrosis induced by anlotinib, we next sought to understand the underlying molecular mechanisms via transcriptome-wide differential gene expression analysis (Fig. 2e). The results suggested that multiple biological processes or signalling pathways are involved in anlotinib-induced cytotoxicity (Fig. 2f, Supplementary Fig. 3). Interestingly, among the down-regulated genes, we found that certain angiogenesis-related biological processes (including angiogenesis, positive regulation of endothelial cell differentiation, and microtubule processes) were the most enriched (Fig. 2f).

CCL2 is an important angiogenesis target for tumour therapy.[20] Here, we found that CCL2 transcription was down-regulated more than 17-fold after anlotinib treatment *in vitro* (Fig. 2g, h). Analysis of the TCGA cohort suggested that high CCL2 expression significantly correlated with reduced survival in NSCLC patients (Supplementary Fig. 4a, b). However, the gene coexpressed with CCL2 in LUAD, IL6, was not associated with anlotinib-induced anti-angiogenesis (Supplementary Fig. 4c-g). Therefore, we performed a series of assays to characterize CCL2 expression *in*

vitro and *in vivo*. CCL2 levels in the medium were significantly decreased after exposure of NSCLC cell lines (NCI-H1975, NCI-H2228, A549, NCI-H1650, and NCI-H2228) to anlotinib (Fig. 2i, Supplementary Fig. 5). CCL2 levels both in serum and tumour tissue also markedly decreased after anlotinib administration (Fig. 2j, k). Based on these observations, we hypothesized that anlotinib-induced anti-angiogenesis might be mainly attributed to the reduced CCL2 content.

Anlotinib inhibits MMP9 expression *in vitro* and *in vivo*

Previous studies have reported that the down-regulation of CCL2 inhibits protein expression of angiogenesis-related signalling pathway *in vitro* and *in vivo*.[20, 21] In the present study, we found that among the MMPs (including MMP1, MMP2, MMP3, MMP9 and MMP19), the mRNA expression of MMP9 was nearly blocked after anlotinib treatment *in vitro* and *in vivo* (Fig. 3a). Moreover, MMP9 protein was markedly decreased after anlotinib treatment (Fig. 3b, c). Thus, proliferation and vascularization were significantly inhibited after anlotinib administration (Fig. 3d-g). Because high MMP9 levels contribute to tumour vascularization,[22] our results suggest that anlotinib-induced anti-angiogenesis possibly attributed to the inhibition of the CCL2-MMP9 axis.

Anlotinib inhibits angiogenesis via the CCL2-MMP9 axis

To further understand the role of CCL2 in anlotinib-induced anti-angiogenesis, human recombinant CCL2 was added to anlotinib-treated NCI-H1975 cells or injected into NCI-H1975-derived xenograft models. We found that exogenous CCL2

dramatically offset anlotinib-induced cytotoxicity (including cell apoptosis induction, cell invasion inhibition, cell cycle arrest, and cell migration inhibition) *in vitro* (Supplementary Fig. 6). Moreover, we evaluated the effect of replenished exogenous CCL2 on angiogenesis-related and proliferation-related proteins in NCI-H1975 *in vitro*, and we found that extrinsic CCL2 markedly recovered the expression levels of MMP9, CD31 and Ki67 (Fig. 4a, b).

For the *in vivo* assessments, we found that both the tumour volume and fold change of tumour volume increased significantly in the anlotinib-treated models injected with CCL2 (Fig. 4c). Moreover, the survival time dramatically declined after CCL2 administration (Fig. 4d). Consistent with the observations *in vitro*, intratumoural MMP9 expression was significantly recovered (Fig. 4e). Importantly, extrinsic CCL2 significantly neutralized anlotinib-induced anti-angiogenesis (Fig. 4f, g). These results indicate that high CCL2 levels not only correlate with vascularization, but also contribute to offsetting the anlotinib-induced angiogenesis block. Collectively, these results demonstrated that anlotinib had an anti-angiogenesis effect via the inhibition of the CCL2-MMP9 axis (Fig. 4h) and suggested that anlotinib-induced CCL2 blockade could be associated with the response to anlotinib in refractory advanced NSCLC patients.

Changes in serum CCL2 levels reflect and predict the anlotinib response in refractory advanced NSCLC patients

Given the active involvement of CCL2 in anlotinib treatment, we next asked

whether the CCL2 levels could be used to predict the response to anlotinib. Among 28 NSCLC patients treated with anlotinib, we found that serum CCL2 levels in responsive patients (n = 14) decreased significantly at BR and increased at PD, with 13 responders showing decreased serum CCL2 levels at BR. In non-responders (n = 14), serum CCL2 levels increased at PD, with 11 non-responders showing increased CCL2 levels (Fig. 5a-c). Moreover, we observed the serum CCL2 levels in responders were markedly high compared with those in non-responders at BL (Supplementary Fig. 7a). Kaplan-Meier analysis suggested that serum CCL2 levels at BL potentially predict tumour response in refractory advanced NSCLC patients during treatment with anlotinib (Supplementary Fig. 7b, c).

As mentioned above, in NSCLC cell lines (Fig. 2g-i, Supplementary Fig. 5), NCI-H1975-derived xenograft model (Fig. 2j, k), and NSCLC patients (Fig. 5b), we observed the remarkable decrease of CCL2 levels upon anotinib treatment. In addition to serum CCL2 levels at BL, we ask whether the change of CCL2 levels could be used to predict anlotinib response. We thus examined the changes in serum CCL2 levels after anlotinib therapy. Surprisingly, we found that early changes in CCL2 levels were clearly associated with the response to anlotinib (Fig. 5d). Subsequently, we used a median cut-off point to assess the anlotinib response. PFS was dramatically longer in NSCLC patients with early decreases in serum CCL2 levels than in those with early increases (Fig. 5e). Similar results were observed when OS analysis was performed in the cohort using this stratification. Compared with NSCLC patients with increased CCL2 levels after anlotinib therapy, the OS of patients with decreased

CCL2 levels was significantly longer (Fig. 5f).

DISCUSSION

As an oral multi-targeted TKI, anlotinib exhibits efficacy in various cancers.[7, 9-12] Our clinical evidence suggests that anlotinib prolongs PFS and OS in patients with refractory advanced NSCLC.[7, 9, 10] Although the clinical trial results suggest that anlotinib potentially has an anti-angiogenesis effect to inhibit disease progression, the underlying molecular mechanism is still unclear. In addition, traditional stratification methods for evaluating or predicting responses to new inhibitors are less efficient for identifying the best responders from NSCLC patients. To address these issues, we sought herein to understand the mechanisms of the anlotinib-induced anti-angiogenesis effect and identify a biomarker that could be used to screen anlotinib responders.

Standard therapeutic regimens have been recommended to advanced NSCLC patients as first-line and second-line agents. Third-line and beyond third-line therapy for refractory advanced NSCLC lack a uniform standard, which has been regarded as an intractable problem for the lung cancer research community. Recently, the National Comprehensive Cancer Network (NCCN) has provided third-line therapy regimens, including chemotherapy and immunotherapy, for refractory advanced NSCLC.[5] However, multi-targeted TKIs are still worth pursuing. We found that anlotinib could be used as an oral multi-target TKI for third-line or beyond third-line therapy in refractory advanced NSCLC patients.[7, 9, 10] Biomarkers play an important role in

drug development for lung cancer therapy. First-generation TKIs provide great benefits to LUAD patients harbouring EGFR mutations (19 deletion or L858R).[23, 24] Advanced NSCLC patients harbouring 50% positive PD1/PDL1 expression or a higher tumour mutation burden (TMB) acquire more benefits from checkpoint inhibitors (such as pembrolizumab, nivolumab and atezolizumab).[25-27] In this study, we found that LUAD patients harbouring driver gene-positive mutations, especially patients harbouring the $EGFR^{T790M}$ mutation, obtained more benefit from anlotinib therapy based on OS analysis rather than PFS analysis. The administration of 3rd generation TKIs (such as AZD9291) or recover sensitivity to 1st TKI may account for major reasons.[28, 29] Although intense efforts have been exerted to identify biomarkers based on known molecular characteristics, it is still difficult to distinguish anlotinib responders from all advanced NSCLC patients.

Understanding the molecular mechanisms of anlotinib could facilitate biomarker identification. Previous studies have indicated that anlotinib selectively inhibits growth factor receptor, including VEGFR (1,2 and 3), PDGFR (α and β), and FGFR (1,2,3 and 4), among others.[8-10, 13, 14] Anlotinib exerts its antitumour effects in tumour cell line-derived xenograft animal models.[8] Furthermore, anlotinib suppresses tumour cell growth through the inhibition of c-Kit, Ret, Aurora-B, c-FMS and DDR1.[15-17] Elevated CCL2 levels in the tumour microenvironment or blood are associated with tumour angiogenesis.[22, 30, 31] CCL2 activation contributes to angiogenesis and metastasis in lung cancer, breast cancer, and pancreatic cancer, among others.[20, 21, 32] The majority of tumours secrete CCL2, a key

pro-angiogenesis factor, to stimulate tumour vascularization and provide nutrition for tumour growth and metastasis.[33, 34] Here, we observed that anlotinib inhibited NCI-H1975 cell proliferation via CCL2 blockade *in vitro* and *in vivo*. Moreover, anlotinib-induced tumour necrosis was attributed to angiogenesis inhibition by blocking the CCL2-MMP9 axis in NCI-H1975-derived xenografts models.

Valuable biomarkers contribute to the prediction of responders to new drugs.[23-27] Thus, the identification of a proper biomarker for distinguishing responders from non-responders to anlotinib is urgent. Here, we observed herein that alterations of serum CCL2 levels were associated with the response to anlotinib therapy in advanced NSCLC. Moreover, we reported that changes in serum CCL2 levels could predict anlotinib responders among refractory advanced NSCLC patients. Although we found serum CCL2 levels at BL would be used to predict anlotinib responder in this study. However, it is reported that plasma CCL2 levels in different cohorts of race, age, and smoking.[35, 36] Considering anlotinib induces a remarkable change of CCL2 levels in NSCLC cell lines (Fig. 2g-i, Supplementary Fig. 5), NCI-H1975-derived xenograft model (Fig. 2j, k), and NSCLC patients (Fig. 5b), we found that the change of CCL2 levels, rather than CCL2 levels themselves, could be used to more effectively predict anlotinib response. And a large-scale prospective study should be performed to evaluate its potential as a biomarker for anlotinib therapy.

CONCLUSIONS

The present study not only reveals an important molecular mechanism of anlotinib-induced anti-angiogenesis via inhibiting the CCL2-MMP9 axis, but also offers insights that serum CCL2 levels could serve as a predictive biomarker for distinguishing anlotinib responders from non-responders in refractory advanced NSCLC patients receiving third-line or beyond third-line therapies.

ACKNOWLEDGEMENTS

The authors thank the patients for their participation, and the investigators for their support. We thank Dr. Xunqiang Wang and Dr. Wei Shi from Chia-tai Tianqing Pharmaceutical Co Ltd for their help and support. This work was supported by the program of system biomedicine innovation center from Shanghai Jiao Tong University (Project No. 15ZH4009); the key program of translational medicine from Shanghai Jiao Tong University School of Medicine (Project No. 15ZH1008); National Natural Science Foundation of China (Project No. 81673015); Chia-tai Tianqing Pharmaceutical Co Ltd; and the project of Science and Technology Commission of Shanghai Municipality (Project No. 16140902700).

AUTHOR CONTRIBUTIONS

Experiments were conceived and designed by B.H. Han, J. Lu, L.M. Lu, K. Li and X.D. Zhao. Clinical trials were performed by B.H. Han, K. Li, H. Zhong, T.Q. Chu, X.Y. Zhang, R. Li, J.Y. Sun and R. Zhong. Preclinical experiments were performed by J. Lu, H. Zhong, Y.Q. Yang, M.S. Alam, J. Wu and X.W. Li. Clinical

analysis, bioinformatics analysis and statistical analysis were performed by J. Lu, X.Y. Zhang, Y.Q. Lou, J.L. Xu, Y.W. Zhang, X.D. Zhao and J. Wu. The manuscript was written by J. Lu, and revised by X.D. Zhao and B.H. Han.

COMPETING FINANCIAL INTERESTS STATEMENT

The authors declare no competing financial interest.

References

1. Zhang Y, Zhang L, Li R, et al. Genetic variations in cancer-related significantly mutated genes and lung cancer susceptibility. Ann Oncol. 2017; 28(7): 1625-30.
2. Torre LA, Bray F, Siegel RL, Ferlay J, Lortet-Tieulent J, Jemal A. Global cancer statistics, 2012. CA Cancer J Clin. 2015; 65(2): 87-108.
3. Grose D, Morrison DS, Devereux G, et al. The impact of comorbidity upon determinants of outcome in patients with lung cancer. Lung Cancer. 2015; 87(2): 186-92.
4. Wistuba, II, Gazdar AF. Lung cancer preneoplasia. Ann Rev Pathol. 2006; 1: 331-48.
5. Ettinger DS, Wood DE, Aisner DL, et al. Non–Small Cell Lung Cancer, Version 5.2017, NCCN Clinical Practice Guidelines in Oncology. J Natl Compr Canc Net. 2017; 15(4): 504-35.
6. Siegel RL, Miller KD, Jemal A. Cancer statistics, 2016. CA Cancer J Clin. 2016; 66(1): 7-30.
7. Han BH, Li K, Wang QM, et al. Efficacy and safety of third-line treatment with anlotinib in patients with refractory advanced non-small-cell lung cancer (ALTER-0303): a randomised, double-blind, placebo-controlled phase 3 study. Lancet Oncol. 2017; 18: S3-S3.
8. Sun Y, Niu W, Du F, et al. Safety, pharmacokinetics, and antitumor properties of anlotinib, an oral multi-target tyrosine kinase inhibitor, in patients with advanced refractory solid tumors. J Hematol.Oncol. 2016; 9(1): 105.

9. Han BH, Li K, Zhao YZ, et al. Anlotinib as a third-line therapy in patients with refractory advanced non-small-cell lung cancer: a multicentre, randomised phase II trial (ALTER0302). Br J Cancer. 2018; doi: 10.1038/bjc.2017.478.

10. Han BH, Li K, Wang QM, et al. Effect of Anlotinib as a Third-Line or Further Treatment on Overall Survival of Patients With Advanced Non–Small Cell Lung Cancer The ALTER 0303 Phase 3 Randomized Clinical Trial. JAMA Oncol. 2018; doi:10.1001/jamaoncol.2018.3039.

11. Sun Y, Chi Y, Tan P, et al. Phase II study of anlotinib for treatment of advanced medullary thyroid carcinoma. *ASCO Publication*. 2016:6015-6015.

12. Chi Y, Sun Y, Cai J, et al. Phase II study of anlotinib for treatment of advanced soft tissues sarcomas. *ASCO Publication*. 2016;11005-11005.

13. Lin B, Song X, Yang D, et al. Anlotinib inhibits angiogenesis via suppressing the activation of VEGFR2, PDGFRbeta and FGFR1. *Gene* 2018; 654: 77-86.

14. Xie C, Wan X, Quan H, et al. Preclinical characterization of anlotinib, a highly potent and selective vascular endothelial growth factor receptor-2 inhibitor. *Cancer Sci*. 2018;109: 1207-19.

15. Ashton S, Song YH, Nolan J, et al. Aurora kinase inhibitor nanoparticles target tumors with favorable therapeutic index in vivo. *Sci Transl Med*. 2016; 8(325): 325ra17.

16. Wang C, Chen J, Cao W, Sun L, Sun H, Liu Y. Aurora-B and HDAC synergistically regulate survival and proliferation of lymphoma cell via AKT, mTOR and Notch pathways. *Eur J Pharmacol*. 2016; 779: 1-7.

17. Ambrogio C, Gomez-Lopez G, Falcone M, et al. Combined inhibition of DDR1 and Notch signaling is a therapeutic strategy for KRAS-driven lung adenocarcinoma. *Nat Med*. 2016; 22(3): 270-7.

18. Lu J, Chen J, Xu N, et al. Activation of AIFM2 enhances apoptosis of human lung cancer cells undergoing toxicological stress. *Toxicol Lett*. 2016; 258: 227-36.

19. Zhang XL, Wu J, Wang J, et al. Integrative epigenomic analysis reveals unique epigenetic signatures involved in unipotency of mouse female germline stem cells. *Genome Biol*. 2016; 17(1): 162.

20. Bonapace L, Coissieux MM, Wyckoff J, et al. Cessation of CCL2 inhibition accelerates breast cancer metastasis by promoting angiogenesis. *Nature*. 2014; 515(7525): 130-3.

21. An J, Xue Y, Long M, Zhang G, Zhang J, Su H. Targeting CCR2 with its antagonist suppresses viability, motility and invasion by downregulating MMP-9 expression in non-small cell lung cancer cells. *Oncotarget*. 2017; 8(24): 39230-40.

22. de Palma M, Biziato D, Petrova TV. Microenvironmental regulation of tumour angiogenesis. *Nat Rev Cancer*. 2017; 17(8): 457-74.

23. Lynch TJ, Bell DW, Sordella R, et al. Activating mutations in the epidermal growth factor receptor underlying responsiveness of non-small-cell lung cancer to gefitinib. *N Engl J Med*. 2004; 350(21): 2129-39.

24. Pao W, Miller V, Zakowski M, et al. EGF receptor gene mutations are common in lung cancers from "never smokers" and are associated with sensitivity of tumors to gefitinib and erlotinib. *Proc Natl Acad Sci USA*. 2004; 101(36): 13306-11.

25. Rizvi NA, Hellmann MD, Snyder A, et al. Cancer immunology. Mutational landscape determines sensitivity to PD-1 blockade in non-small cell lung cancer. *Science*. 2015; 348(6230): 124-8.

26. Brahmer J, Reckamp KL, Baas P, et al. Nivolumab versus Docetaxel in Advanced Squamous-Cell Non-Small-Cell Lung Cancer. *N Engl J Med*. 2015; 373(2): 123-35.

27. Herbst RS, Baas P, Kim DW, et al. Pembrolizumab versus docetaxel for previously treated, PD-L1-positive, advanced non-small-cell lung cancer (KEYNOTE-010): a randomised controlled trial. *Lancet.* 2016; 387(10027): 1540-50.

28. Parra HJS, Noto L, Galetta D, et al. A phase II, noncomparative, open label, multicentre, study of AZD9291 in patients with locally advanced or metastatic EGFR mutated "T790M undetectable or unknown" non-small cell lung cancer (stage IIB-IV) after no immediate prior EGFR TKI (OSIRIS study). *J Clin Oncol*.2017: 35.

29. Chang GC, Tseng CH, Hsu KH, et al. Predictive factors for EGFR-tyrosine kinase inhibitor retreatment in patients with EGFR-mutated non-small-cell lung cancer - A multicenter retrospective SEQUENCE study. *Lung Cancer.*2017: 104: 58-64.

30. Fridlender ZG, Buchlis G, Kapoor V, et al. CCL2 blockade augments cancer immunotherapy. *Cancer Res.* 2010; 70(1): 109-18.

31. Devaud C, John LB, Westwood JA, Darcy PK, Kershaw MH. Immune modulation of the tumor microenvironment for enhancing cancer immunotherapy. *Oncoimmunology.* 2013; 2(8): e25961.

32. Sanford DE, Belt BA, Panni RZ, et al. Inflammatory monocyte mobilization decreases patient survival in pancreatic cancer: a role for targeting the CCL2/CCR2 axis. *Clin Cancer Res.* 2013; 19(13): 3404-15.

33. Tas SW, Maracle CX, Balogh E, Szekanecz Z. Targeting of proangiogenic signalling pathways in chronic inflammation. *Nat Rev Rheumatol.* 2016; 12(2): 111-22.

34. Kudo-Saito C, Shirako H, Ohike M, Tsukamoto N, Kawakami Y. CCL2 is critical for immunosuppression to promote cancer metastasis. *Clin Exp Metastas.* 2013; 30(4): 393-405.

35. McDermott DH, Yang Q, Kathiresan S, et al. CCL2 polymorphisms are associated with serum

monocyte chemoattractant protein-1 levels and myocardial infarction in the framingham heart study. *Circulation.*2005; 112(8): 1113-20.

36. Bielinski SJ, Pankow JS, Miller MB, et al. Circulating MCP-1 levels shows linkage to chemokine receptor gene cluster on chromosome 3: the NHLBI Family Heart Study follow-up examination. *Genes Immun.*2007; 8(8): 684-90.

Figure legends

Figure 1. A retrospective analysis of anlotinib Phase III clinical trial indicates that the overall survival of LUAD patients is associated with the driver gene mutation type. (a) Timeline of the anlotinib Phase III clinical trial. (b, c) Kaplan-Meier plots of PFS and OS in NSCLC patients receiving anlotinib therapy by negative (n = 147) and positive (n = 93) driver gene mutations. Median PFS: 147 days (95% CI 131-163) vs 166 days (95% CI 143-189), median OS: 259 days (95% CI 234-284) vs 364 days (95% CI 332-396). (d, e) Analysis of PFS and OS in anlotinib-treated LUAD patients harbouring EGFR and other positive mutations. (f, g) Kaplan-Meier plots of PFS and OS in driver gene-positive LUAD patients receiving anlotinib therapy by $EGFR^{T790M}$-negative (n = 84) and $EGFR^{T790M}$-positive (n = 9) mutations. Median PFS: 166 days (95% CI 144-188) vs 182 days (95% CI 53-311), median OS: 332 days (95% CI 299-365) vs Undefined.

Figure 2. Transcriptome analysis indicates that anlotinib-induced CCL2 blockade is associated with anlotinib-induced anti-angiogenesis. (a) Timeline of the experiments *in vivo*. (b) Measurements of subcutaneous tumour volumes in the Ctrl and anlotinib groups. Assessment of the fold change in tumour growth. Bars = mean ± SD, n = 9, $^{**}P < 0.01$. (c) Kaplan–Meier survival curves of mice treated with Ctrl, anlotinib (1.5 mg/kg) and anlotinib (2.25 mg/kg), respectively. n = 9, $^{***}P < 0.001$. (d) Representative images of H&E staining of NCI-H1975-derived xenograft

tumours at 22 days after treatment with anlotinib versus Ctrl. Images were obtained at 10×, and the scale bars are 25 μm. Three views of one section per animal; n = 9 mice per group. (e) Flow diagram for identifying up-regulated and down-regulated genes from transcriptomes of the Ctrl versus anlotinib. (f) Functional enrichment of anlotinib-induced up-regulated and down-regulated genes by GO analysis. There were 1128 down-regulated genes (fold change > 2) and 636 up-regulated genes (fold change > 2) subjected to GO analysis. (g) The top 10 down-regulated genes after anlotinib treatment in NCI-H1975 cells. (h, i) NCI-H1975 cells were exposed to anlotinib (8 μg/ml) for 24 hours. mRNA expression of CCL2 was detected by RT-qPCR. Bars = mean ± SD, n = 3, ***P< 0.001. CCL2 levels in the medium were evaluated using an ELISA kit. Bars = mean ± SD, n = 4, ***P< 0.001. (j) CCL2 levels in serum from NCI-H1975 tumour-bearing nude mice during anlotinib treatment (Day 5, Day 10, and Day22). Bars = mean ± SD, n = 9, ***P< 0.001. (k) CCL2 levels in the tumour homogenate from NCI-H1975-derived xenograft tumours on Day 22. Bars = mean ± SD, n = 9, ***P< 0.001.

Figure 3. Anlotinib inhibits NCI-H1975 cell-derived angiogenesis *in vitro* and *in vivo*. (a) MMP mRNA expressions in anlotinib-treated (8 μg/ml) NCI-H1975 cells and anlotinib-treated (2.25 mg/kg) NCI-H1975-derived xenografts tumours. Bars = mean ± SD, n = 3. (b) Representative images of MMP9-stained NCI-H1975 cells with or without anlotinib (4 μg/ml) administration. Images were obtained at 10×, and the scale bars are 100 μm. Eight images per group. (c) Representative images of MMP9-stained NCI-H1975-derived xenograft tumour tissues after anlotinib (2.25

mg/kg) treatment for 22 days. Three views of one section per animal. Bars = mean ± SD, n = 9 mice per group, ***P< 0.001. Images were obtained at 20×, and the scale bars are 50 μm. (d) mRNA expression of *MKI67* and *PECAM1*was evaluated by RT-qPCR after anlotinib (8 μg/ml) treatment *in vitro*. Bars = mean ± SD, n = 3, **P< 0.01, ***P< 0.001. (e) Representative images of CD31 and Ki67 expression in anlotinib-treated (2 μg/ml) NCI-H1975 cells. CD31 labelled with FITC (green) and Ki67 labelled with PI (red). Five images per group. Scale bars: 25 μm. (f, g) Representative images of Ki67-stained and CD31-stained NCI-H1975-derived xenograft tumour tissue after anlotinib (2.25 mg/kg) treatment for 22 days. Three views of one section per animal. Bars = mean ± SD, n = 9 mice per group, **P< 0.01. Ki67: images were obtained at 10×, and the scale bars are 100 μm. CD31: images were obtained at 20×, and the scale bars are 25 μm.

Figure 4. Replenishment of exogenous CCL2 recovers anlotinib-induced anti-angiogenesis *in vitro* and *in vivo*. NCI-H1975 cells were exposed to CCL2 (50 ng/ml) and anlotinib (6 μg/ml), alone or together, for 24 hours. (a) Representative images of MMP-9 expression. Eight images per group. Scale bars: 20 μm. (b) Representative images of CD31 and Ki67 expression. CD31 labelled with FITC (green) and Ki67 labelled with PI (red). Six images per group. Scale bars: 100 μm. (c) Measurement of subcutaneous tumour volumes of Ctrl, anlotinib (2.5 mg/kg) and anlotinib (2.5 mg/kg) + CCL2 (5 μg/kg, iv, qod). Bars = mean ± SD, n = 9, *P< 0.05, ***P< 0.001. (d) Kaplan–Meier survival curves of mice treated with Ctrl, anlotinib and anlotinib plus CCL2, respectively. n = 9, ***P< 0.001. (e-g) Representative

images of MMP9-stained, CD31-stained and lectin-stained NCI-H1975-derived xenograft tumour tissues on day 22. Three views of one section per animal. Bars = mean ± SD, n = 9 mice per group, $^{**}P < 0.01$, $^{***}P < 0.001$. Images were obtained at 20×, and the scale bars are 50 μm. (h) Schematic of anlotinib inhibition of angiogenesis via blocking the CCL2-MMP9 axis. Tumour cells secrete CCL2 into the tumour microenvironment. CCL2 activates MMP9 expression and then promotes neovascularization. Administration of anlotinib blocks the CCL2-MMP9 axis in NCI-H1975 cells and NCI-H1975-derived xenografts, contributing to the inhibition of angiogenesis.

Figure 5. Changes in serum CCL2 levels are associated with PFS and OS in refractory advanced NSCLC patients treated with anlotinib. Advanced NSCLC patients were treated with anlotinib, and serum CCL2 levels were evaluated at baseline (BL), at best response (BR), and at progressive disease (PD). (a) The alterative pattern of CCL2 levels in anlotinib-responsive and anlotinib-non-responsive NSCLC patients. n = 14, $^{*}P < 0.05$. (b) Serum CCL2 levels at different time-points in anlotinib-responsive NSCLC patients (n = 14). (c) Serum CCL2 levels were plotted at BL and PD time-points for anlotinib-non-responsive NSCLC patients (n = 14). (d) Percentages of changes in serum CCL2 in advanced NSCLC patients treated with anlotinib, from baseline to 2 months. Bars = mean ± SD, n = 14, $^{***}P < 0.001$. (e) Kaplan-Meier plots of PFS stratified by the changes in CCL2 levels in advanced NSCLC patients treated with anlotinib. n = 28, cut-off-high: 50%; cut off-low: 50%, median PFS: 189 days (95% CI 131-247) vs 35.5 days (95% CI 25-46), log rank P <

0.001. (f) Kaplan-Meier plots of OS stratified by the changes in CCL2 levels in advanced NSCLC patients treated with anlotinib. n = 28, cut-off-high: 50%; cut off-low: 50%, median OS: 378 days (95% CI 306-451) vs 158.5 days (95% CI 110-243), log rank $P < 0.001$.

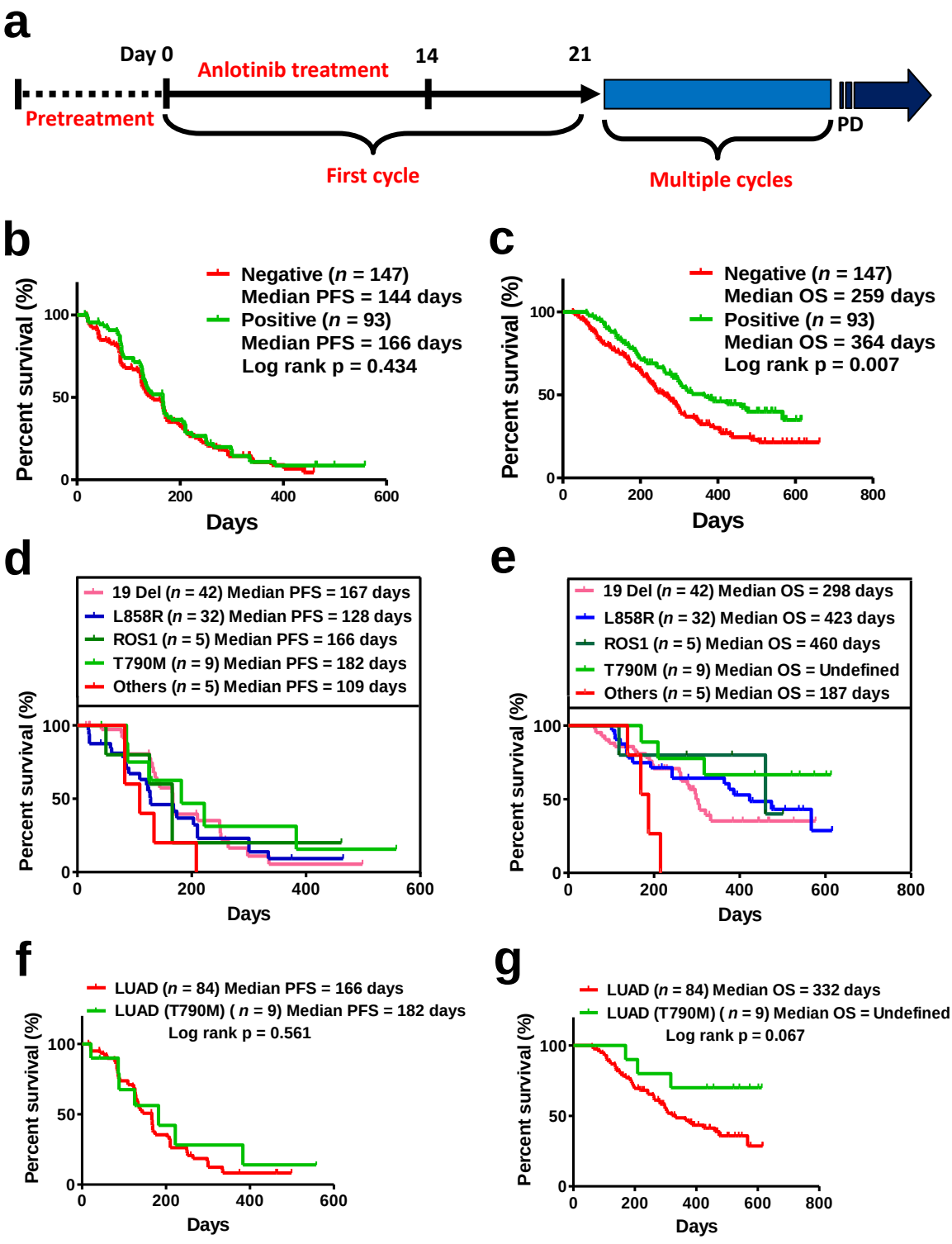
a
Day 0
Anlotinib treatment
14
21
Pretreatment
PD
First cycle
Multiple cycles
b
Negative (n = 147)
Median PFS = 144 days
Positive (n = 93)
Median PFS = 166 days
Log rank p = 0.434
Percent survival (%)
Days
c
Negative (n = 147)
Median OS = 259 days
Positive (n = 93)
Median OS = 364 days
Log rank p = 0.007
Percent survival (%)
Days
d
19 Del (n = 42) Median PFS = 167 days
L858R (n = 32) Median PFS = 128 days
ROS1 (n = 5) Median PFS = 166 days
T790M (n = 9) Median PFS = 182 days
Others (n = 5) Median PFS = 109 days
Percent survival (%)
Days
e
19 Del (n = 42) Median OS = 298 days
L858R (n = 32) Median OS = 423 days
ROS1 (n = 5) Median OS = 460 days
T790M (n = 9) Median OS = Undefined
Others (n = 5) Median OS = 187 days
Percent survival (%)
Days
f
LUAD (n = 84) Median PFS = 166 days
LUAD (T790M) (n = 9) Median PFS = 182 days
Log rank p = 0.561
Percent survival (%)
Days
g
LUAD (n = 84) Median OS = 332 days
LUAD (T790M) (n = 9) Median OS = Undefined
Log rank p = 0.067
Percent survival (%)
Days

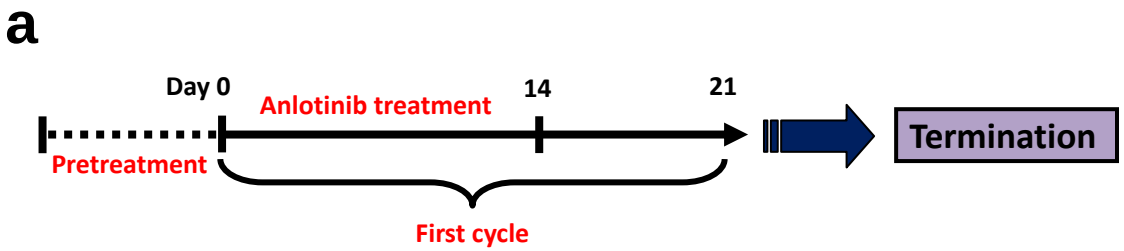

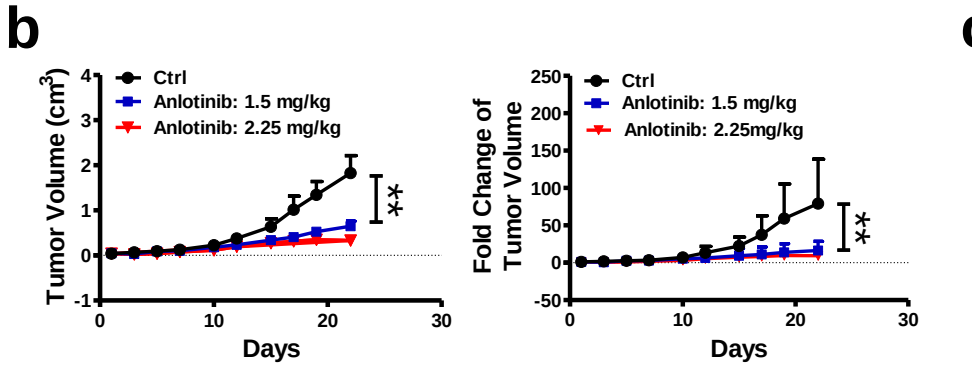

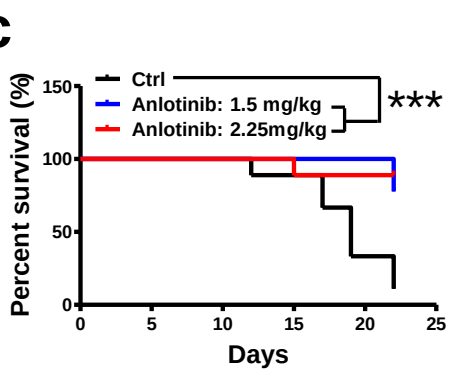

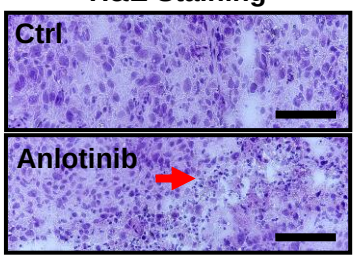

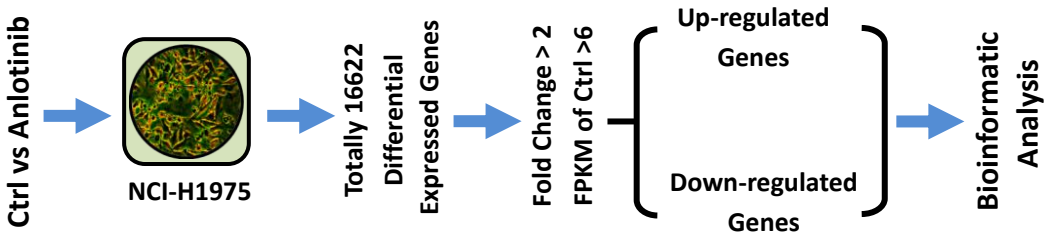

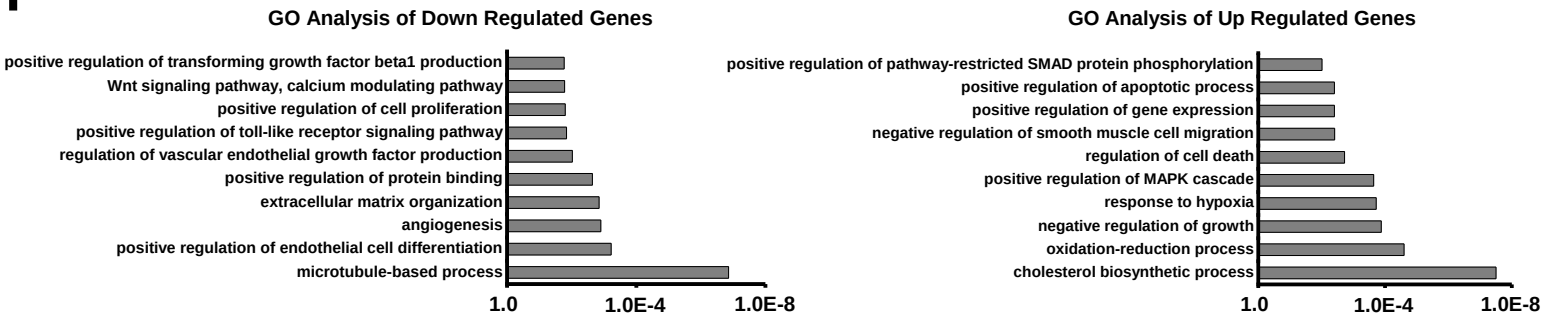

g

Gene name	Log2 (fold change)	P-value
CCL2	-4.11297	1.59E-02
SERPINB4	-3.20408	1.50E-03
TUBA4A	-2.87329	5.00E-05
STRA6	-2.81923	9.00E-04
COL7A1	-2.55164	5.00E-05
AQP3	-2.45409	6.75E-03
CXCL2	-2.29888	1.08E-02
MB	-2.2613	6.60E-03
NBPF16	-2.24777	7.00E-04
HIST1H3G	-2.08321	1.09E-02

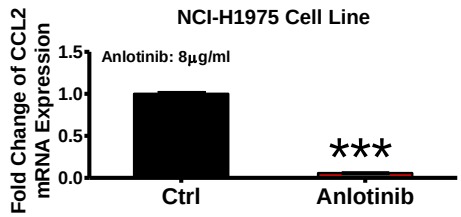

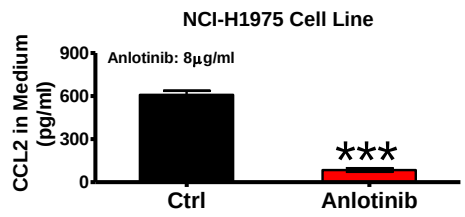

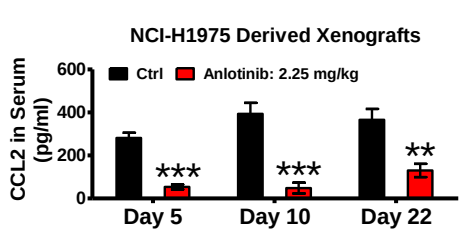

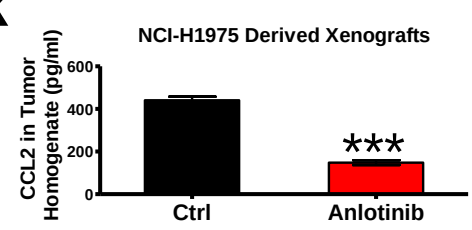

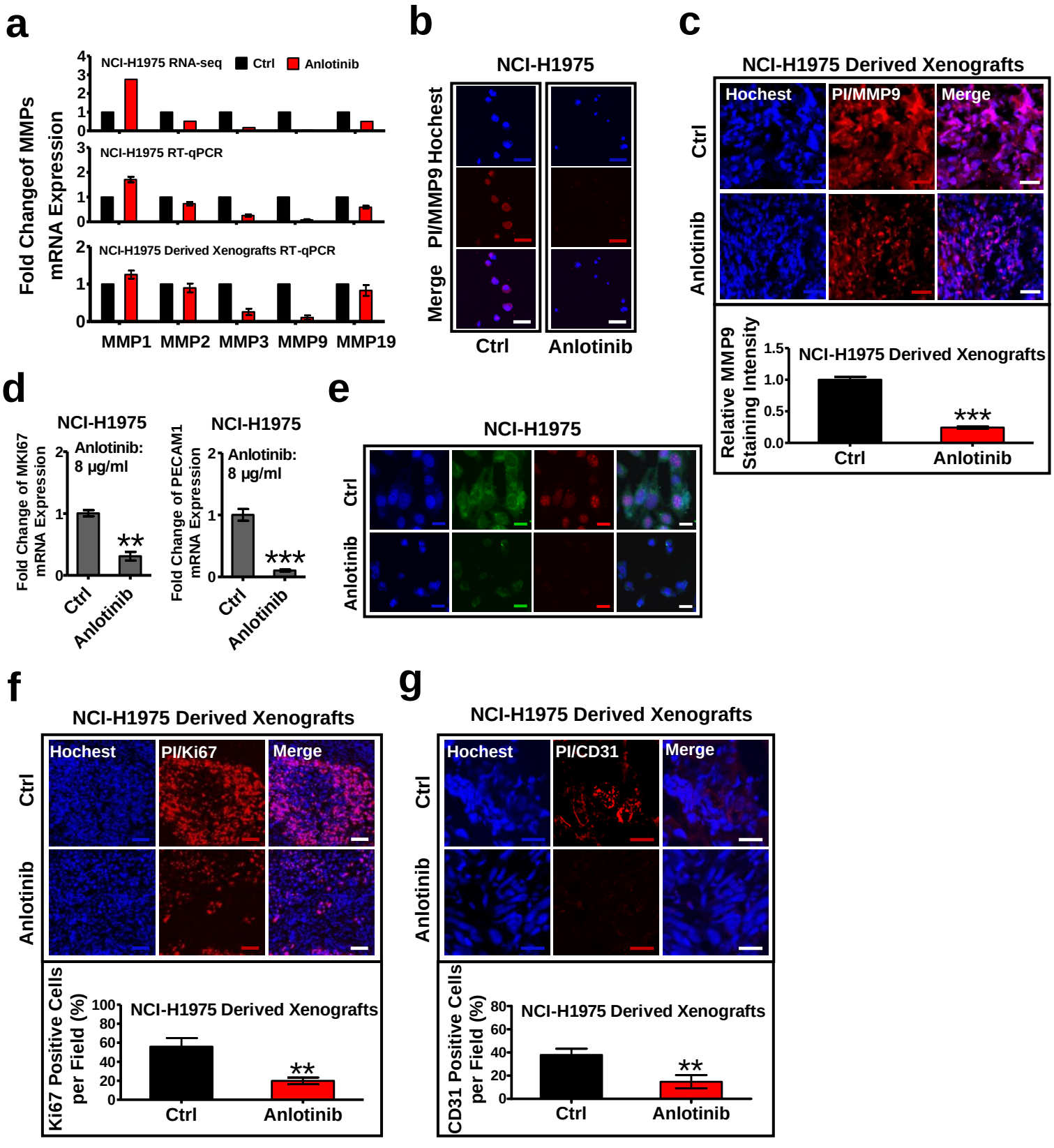
a
NCI-H1975 RNA-seq
Ctrl
Anlotinib
NCI-H1975 RT-qPCR
NCI-H1975 Derived Xenografts RT-qPCR
Fold Changeof MMPs mRNA Expression
MMP1
MMP2
MMP3
MMP9
MMP19
b
NCI-H1975
PI/MMP9
Hochest
Merge
Ctrl
Anlotinib
c
NCI-H1975 Derived Xenografts
Hochest
PI/MMP9
Merge
Ctrl
Anlotinib
Relative MMP9 Staining Intensity
NCI-H1975 Derived Xenografts
***
d
NCI-H1975
Fold Change of MKI67 mRNA Expression
Anlotinib: 8 μg/ml
**
Fold Change of PECAM1 mRNA Expression
***
e
NCI-H1975
f
NCI-H1975 Derived Xenografts
PI/Ki67
Ki67 Positive Cells per Field (%)
g
NCI-H1975 Derived Xenografts
PI/CD31
CD31 Positive Cells per Field (%)

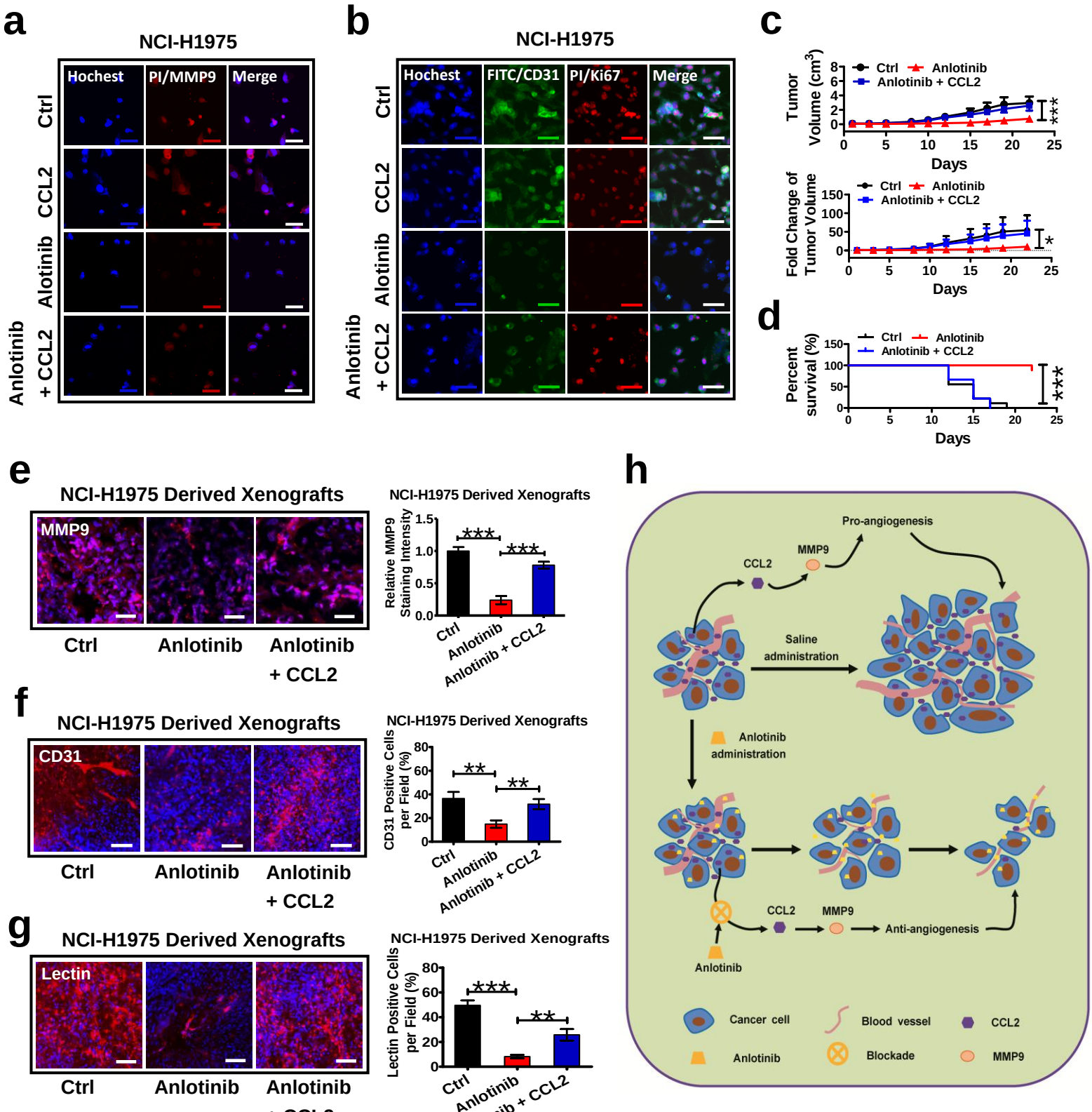
a
NCI-H1975
Hochest
PI/MMP9
Merge
Ctrl
CCL2
Alotinib
Anlotinib + CCL2
b
NCI-H1975
Hochest
FITC/CD31
PI/Ki67
Merge
Ctrl
CCL2
Alotinib
Anlotinib + CCL2
c
Tumor Volume (cm3)
Ctrl
Anlotinib
Anlotinib + CCL2
Days
Fold Change of Tumor Volume
d
Percent survival (%)
e
NCI-H1975 Derived Xenografts
MMP9
Ctrl
Anlotinib
Anlotinib + CCL2
Relative MMP9 Staining Intensity
f
CD31
CD31 Positive Cells per Field (%)
g
Lectin
Lectin Positive Cells per Field (%)
h
Pro-angiogenesis
MMP9
CCL2
Saline administration
Anlotinib administration
Anti-angiogenesis
Cancer cell
Blood vessel
Blockade

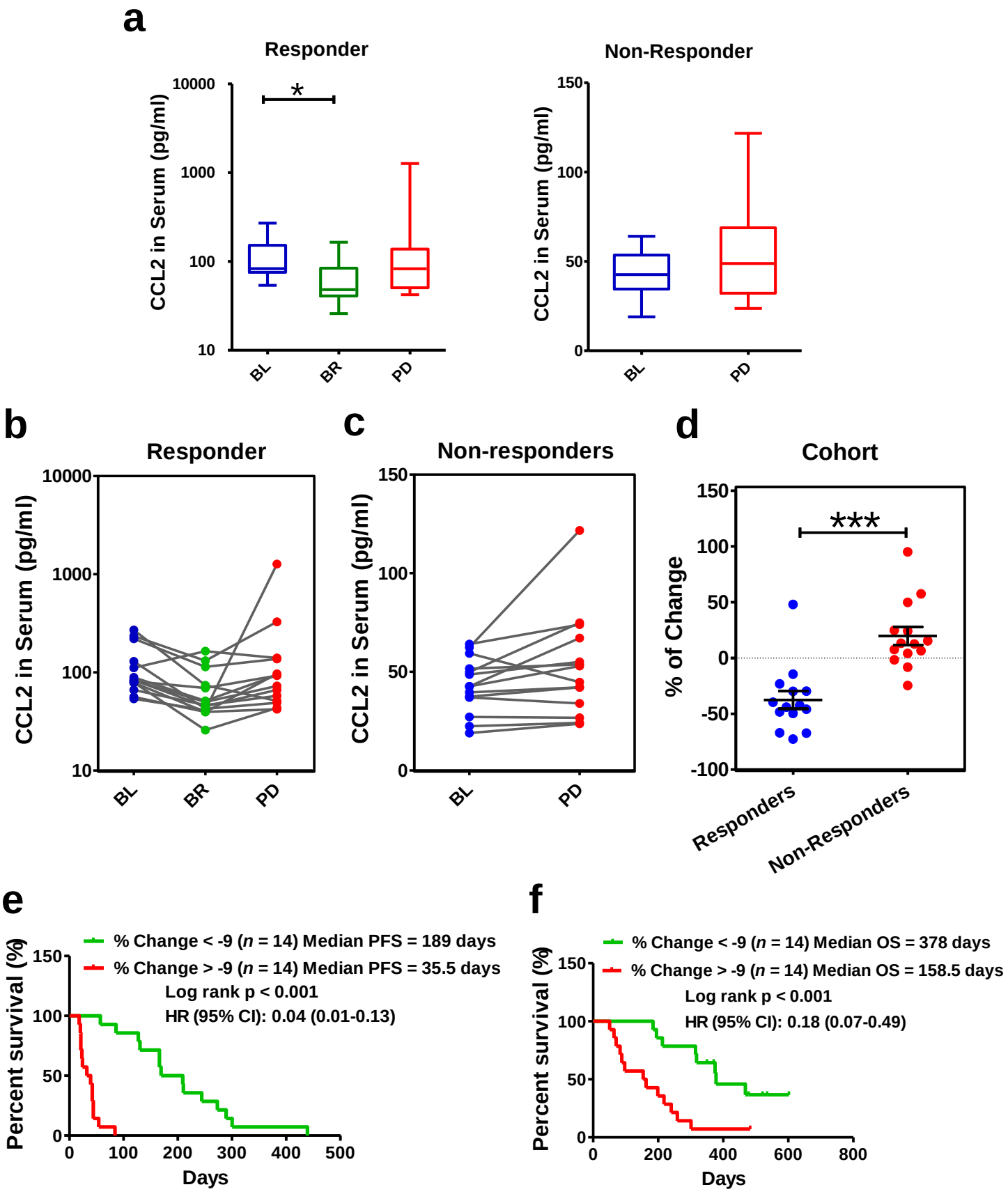
a
Responder
Non-Responder
CCL2 in Serum (pg/ml)
10000
1000
100
10
150
100
50
0
*
BL
BR
PD
b
Responder
c
Non-responders
d
Cohort
% of Change
***
Responders
Non-Responders
e
% Change < -9 (n = 14) Median PFS = 189 days
% Change > -9 (n = 14) Median PFS = 35.5 days
Log rank p < 0.001
HR (95% CI): 0.04 (0.01-0.13)
Percent survival (%)
Days
f
% Change < -9 (n = 14) Median OS = 378 days
% Change > -9 (n = 14) Median OS = 158.5 days
Log rank p < 0.001
HR (95% CI): 0.18 (0.07-0.49)

Supplementary Table 1

Status of NSCLC patients consisted of Anlotinib responder and Anlotinib nonresponder at their first biopsy.

Patients	Age	Gender	Smoking history	Type	Driver gene mutation	Number of Metastases
Responder 1	58	Female	Never	LUAD	$EGFR^{Exon\ 19\text{-}del,\ T790M}$(+)	≤ 3
Responder 2	42	Male	Never	LUAD	ROS(+)	≤ 3
Responder 3	57	Female	Never	LUAD	$EGFR^{L858R}$(+)	≤ 3
Responder 4	49	Female	Never	LUAD	Negative	≤ 3
Responder 5	52	Male	Never	LUAD	Negative	≤ 3
Responder 6	69	Male	Current/former	LUAD	Negative	≤ 3
Responder 7	62	Male	Never	LUAD	$EGFR^{L858R}$(+)	> 3
Responder 8	52	Female	Never	LUAD	Negative	> 3
Responder 9	58	Male	Current/former	LUAD	$EGFR^{Exon\ 19\text{-}del}$ (+)	≤ 3
Responder 10	42	Male	Never	LUAD	Negative	≤ 3
Responder 11	66	Male	Current/former	LUSC	Negative	≤ 3
Responder 12	37	Male	Current/former	LUAD	Negative	> 3
Responder 13	52	Female	Never	LUSC	Negative	≤ 3
Responder 14	58	Female	Never	LUSC	Negative	> 3
Non-Responder 1	62	Male	Never	LUAD	Negative	> 3
Non-Responder 2	57	Male	Current/former	LUSC	Negative	> 3
Non-Responder 3	44	Female	Never	LUAD	Negative	≤ 3
Non-Responder 4	68	Male	Never	LUSC	Negative	≤ 3
Non-Responder 5	68	Male	Never	LUSC	Negative	≤ 3
Non-Responder 6	58	Male	Current/former	LUAD	Negative	> 3
Non-Responder 7	51	Male	Never	LUSC	$EGFR^{L858R}$(+)	≤ 3
Non-Responder 8	50	Male	Current/former	LUAD	Negative	≤ 3
Non-Responder 9	52	Female	Never	LUAD	$EGFR^{Exon\ 19\text{-}del}$ (+)	> 3
Non-Responder 10	59	Female	Never	LUAD	Negative	> 3
Non-Responder 11	48	Female	Never	LUAD	Negative	≤ 3
Non-Responder 12	53	Female	Never	LUAD	Negative	> 3
Non-Responder 13	58	Female	Never	LUAD	Negative	> 3
Non-Responder 14	39	Male	Never	LUSC	Negative	≤ 3

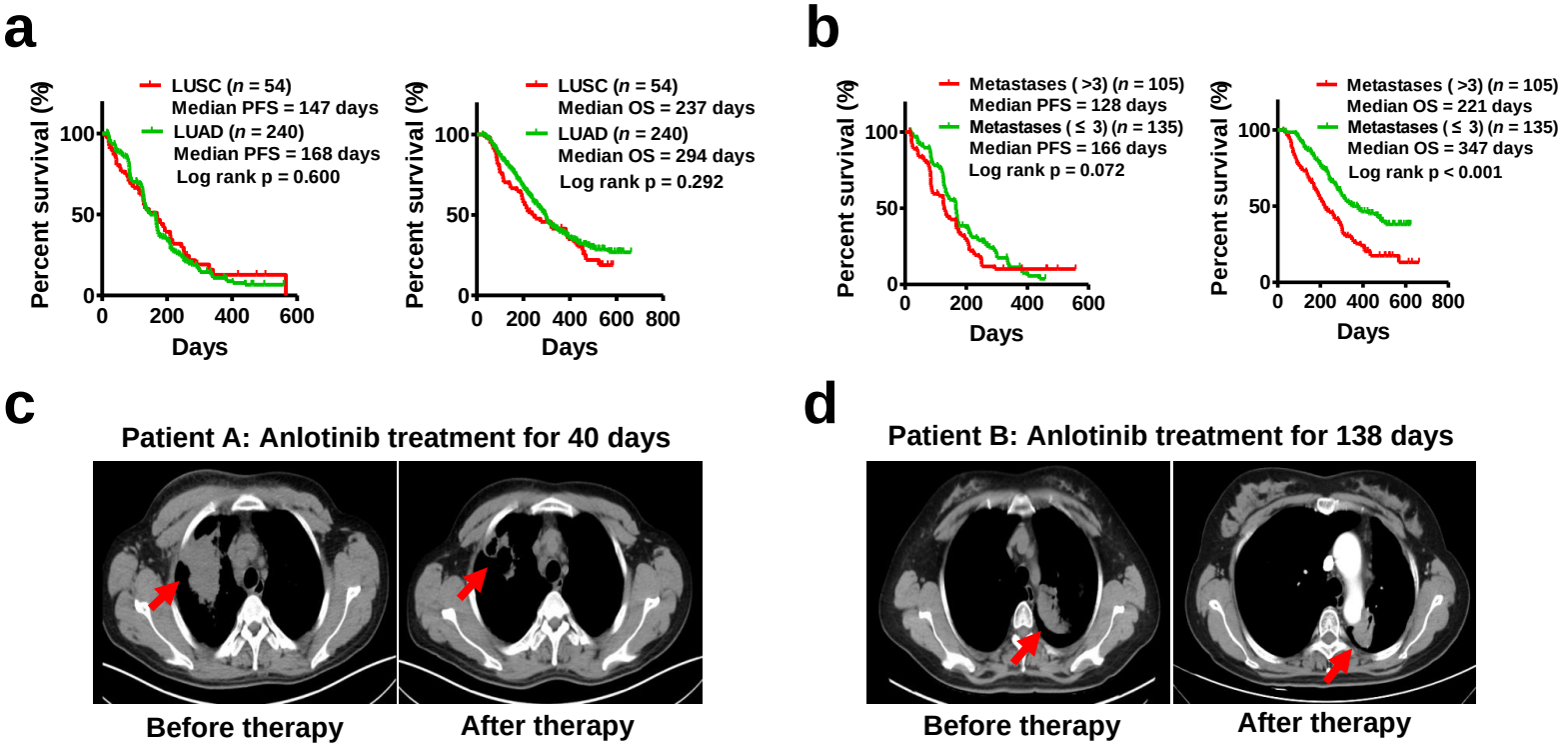

e

Patient ID	Age	Gender	Smoking status	Pathology	EGFR/ALK/ROS1	First-line chemotherapy	Second-line chemotherapy
Patient A	49	Men	Smoker	Adenocarcinoma	- / - / -	AC	DP
Patient B	51	Women	Non-smoker	Adenocarcinoma	- / - / -	NP	AC

Supplementary Figure 1. Anlotinib response stratification analysis performed based on pathological types and number of metastases. (a) Kaplan-Meier plots of PFS and OS in NSCLC patients receiving anlotinib therapy by LUSC (*n* = 54) and LUAD (*n* = 240). Median PFS: 147 days (95% CI 111-183) vs 168 days (95% CI 155-181), median OS: 237 days (95% CI 191-283) vs 294 days (95% CI 274-314). (b) Kaplan-Meier plots of PFS in LUAD patients receiving anlotinib therapy by metastases > 3 (*n* = 105) and metastases ≤ 3 (*n* = 135). Median PFS: 128 days (95% CI 107-149) vs 166 days (95% CI 149-183), median OS: 221 days (95% CI 192-250) vs 347 days (95% CI 321-373). **Anlotinib therapy shrinks the tumour volume in**

refractory advanced LUAD patients without the driver gene mutation. (c, d) Two patients received anlotinib for 40 days and 138 days, respectively. The tumour of Patient A shrank significantly after 40 days of therapy, and the tumour of Patient B showed a partial response after 138 days of therapy. All images represent the maximum diameter of tumours. (e) Clinical characteristics of the two patients with advanced LUAD. AC regimen: pemetrexed plus carboplatin; DP regimen: docetaxel plus cisplatin; NP regimen: vinorelbine plus cisplatin; AC regimen: pemetrexed plus cisplatin.

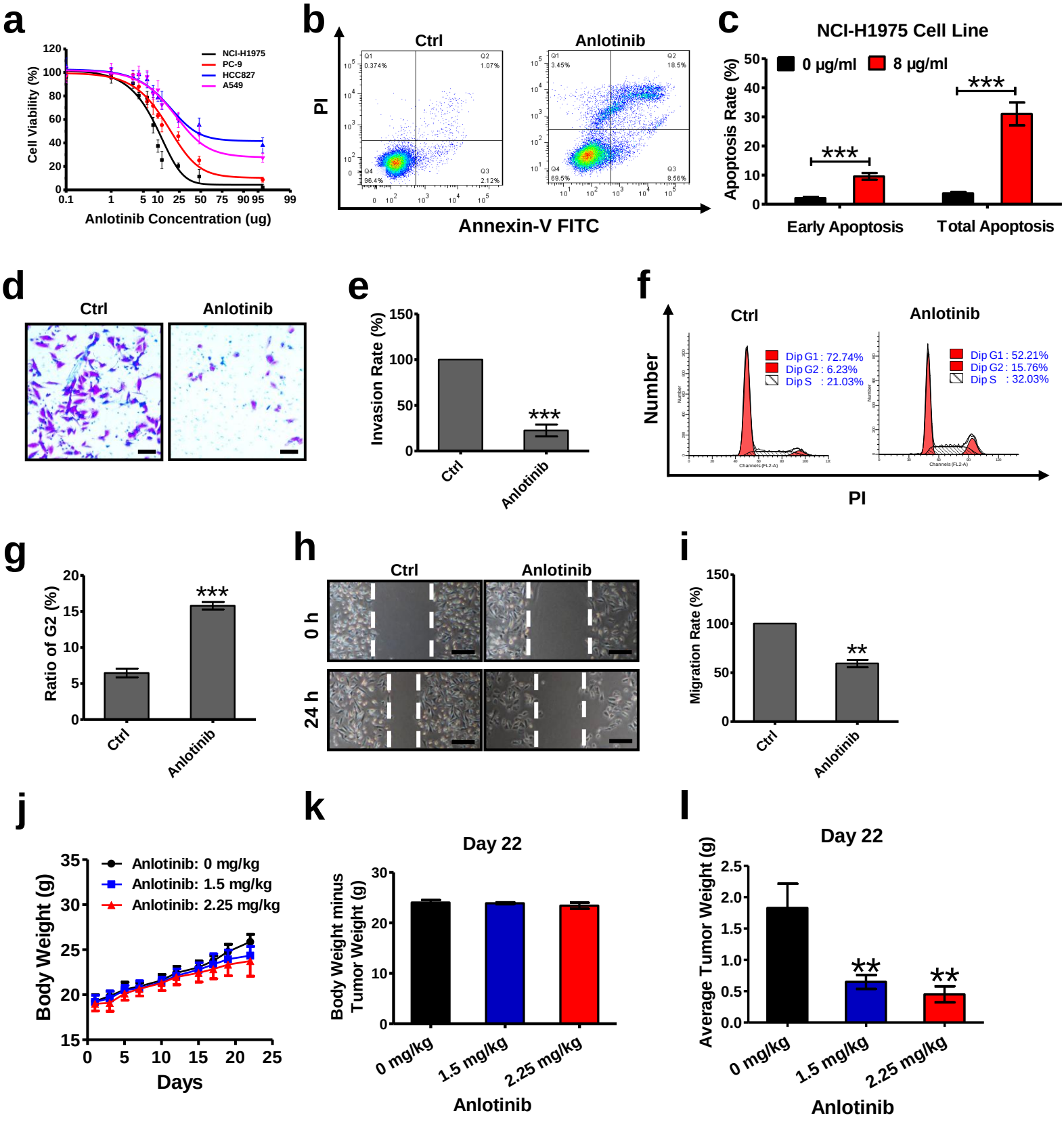
a
Cell Viability (%)
NCI-H1975
PC-9
HCC827
A549
Anlotinib Concentration (ug)
b
Ctrl
Anlotinib
PI
Annexin-V FITC
c
NCI-H1975 Cell Line
0 μg/ml
8 μg/ml
Apoptosis Rate (%)
***
Early Apoptosis
Total Apoptosis
d
Ctrl
Anlotinib
e
Invasion Rate (%)
***
Ctrl
Anlotinib
f
Ctrl
Anlotinib
Number
Dip G1 : 72.74%
Dip G2 : 6.23%
Dip S : 21.03%
Dip G1 : 52.21%
Dip G2 : 15.76%
Dip S : 32.03%
PI
g
Ratio of G2 (%)
***
Ctrl
Anlotinib
h
Ctrl
Anlotinib
0 h
24 h
i
Migration Rate (%)
**
Ctrl
Anlotinib
j
Body Weight (g)
Anlotinib: 0 mg/kg
Anlotinib: 1.5 mg/kg
Anlotinib: 2.25 mg/kg
Days
k
Day 22
Body Weight minus Tumor Weight (g)
0 mg/kg
1.5 mg/kg
2.25 mg/kg
Anlotinib
l
Day 22
Average Tumor Weight (g)
**
**
0 mg/kg
1.5 mg/kg
2.25 mg/kg
Anlotinib

Supplementary Figure 2. Anlotinib-induced NCI-H1975 cell cytotoxic effects *in vitro* and *in vivo*. (a) Cell viabilities were evaluated by CCK8 after LUAD cell line exposure to Anlotinib for 24 hours. Bars = mean ± SD, $n = 3$. (b, c) NCI-H1975 cells were exposed to anlotinib (8 μg/ml) for 24 hours, and then, flow cytometry was used to detect apoptotic. Analyses of early apoptosis and total apoptosis were performed based on flow cytometric detection. Bars = mean ± SD, $n = 3$, ***$P < 0.001$. (d, e) Transwell assays to assess NCI-H1975 cell invasion with or without anlotinib (2 μg/ml) treatment. The invasion rate was calculated based on the transwell assays. Bars = mean ± SD, $n = 3$, ***$P < 0.001$. (f, g) NCI-H1975 cells were exposed to anlotinib (6 μg/ml) for 24 hours, and then, flow cytometry was used to detect the cell cycle distribution. The ratio of G2 was calculated based on flow cytometric detection. Bars = mean ± SD, $n = 3$, ***$P < 0.001$. (h, i) NCI-H1975 cells were exposed to anlotinib (6 μg/ml) for 24 hours, and the wound-healing scratch assay was performed to evaluate proliferation and migration. Bars = mean ± SD, $n = 3$, **$P < 0.01$. (j) Body weight was measured throughout the animal experiment. Bars = mean ± SD, $n = 9$. (k) Body weight minus tumour weight was analysed at the end of the experiment. Bars = mean ± SD, $n = 9$. (l) Measurement of tumour weight at the end of the experiment. Bars = mean ± SD, $n = 9$, **$P < 0.01$.

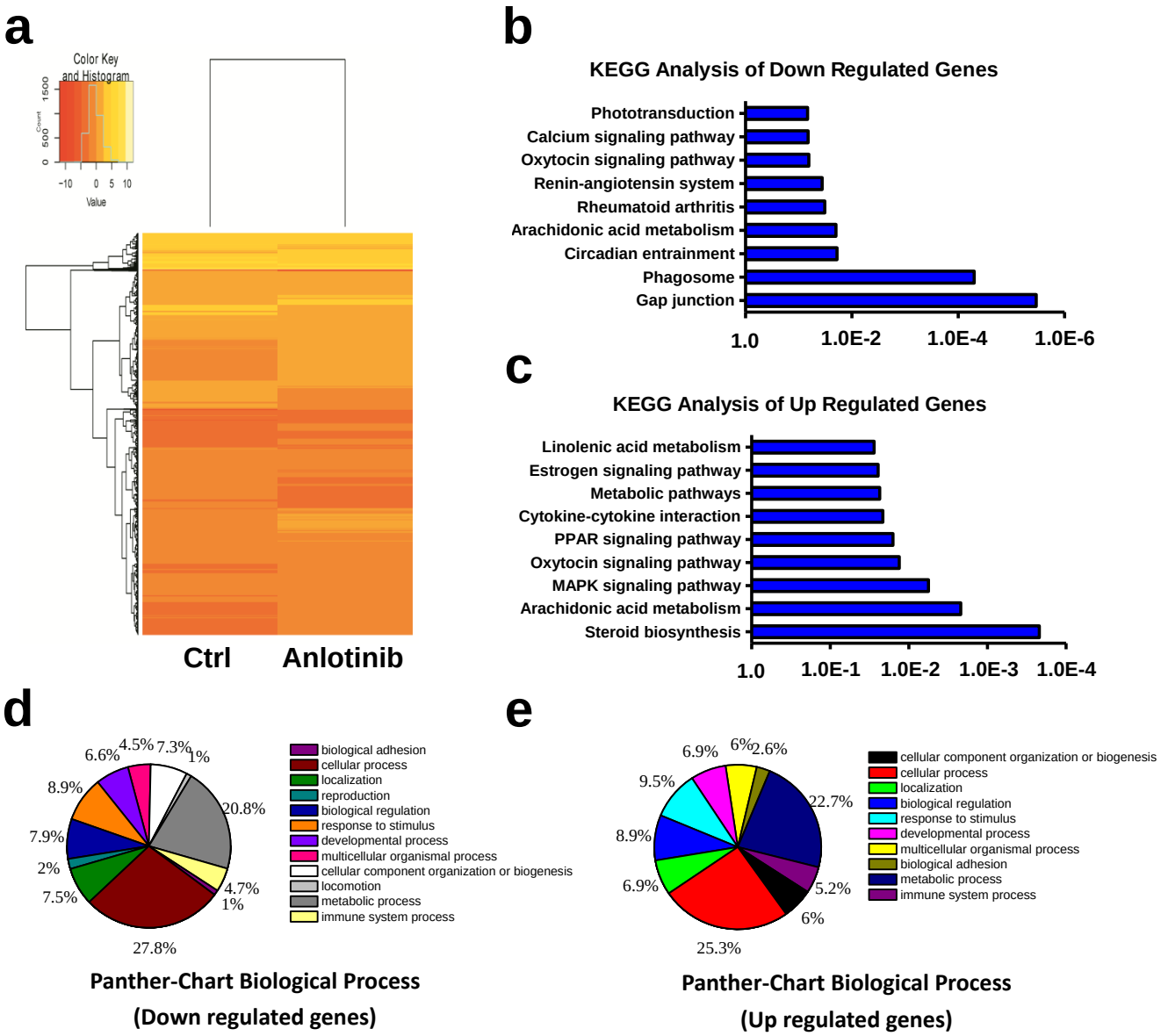

Supplementary Figure 3. Multiple signalling pathways and biological processes are disturbed after treatment with anlotinib (8 μg/ml) in NCI-H1975 cells. (a) Heat map representation of differentially expressed genes in control-treated and anlotinib-treated NCI-H1975 cells. Red represents gene up-regulation, and blue represents gene down-regulation. (b, c) KEGG analysis of differentially expressed genes in the Ctrl vs. anlotinib. There were 1128 down-regulated genes (fold change > 2) and 636 up-regulated genes (fold change > 2) subjected to KEGG analysis. (d, e) Panther analysis of differentially expressed genes in the Ctrl vs. anlotinib. There were 1128 down-regulated genes (fold change > 2) and 636 up-regulated genes (fold change > 2) subjected to Panther analysis.

a

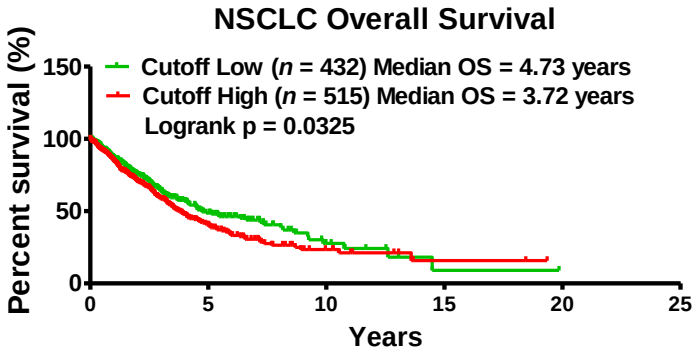

b

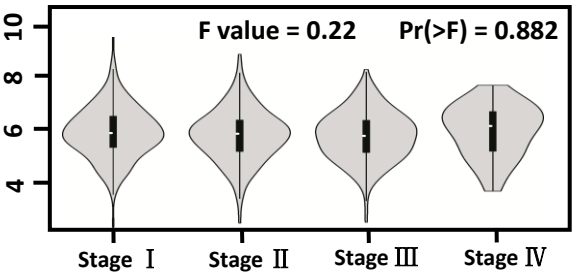

c

Gene Symbol	Gene ID	PCC
IL6	ENSG00000136244.11	0.82
CTD-2369P2.8	ENSG00000267607.1	0.75
RP11-79H23.3	ENSG00000261618.1	0.74
MMP19	ENSG00000123342.15	0.73
ARID5A	ENSG00000196843.15	0.73
SELE	ENSG00000007908.15	0.72
KDM6B	ENSG00000132510.10	0.68
ADAMTS4	ENSG00000158859.9	0.68
RP11-439L18.1	ENSG00000232618.1	0.68
RP11-64B16.2	ENSG00000213144.2	0.68

d

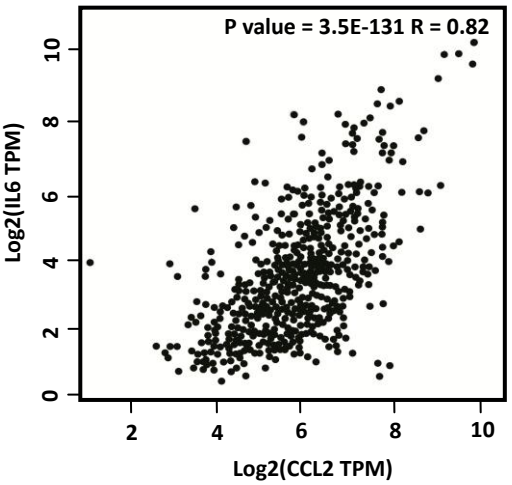

e

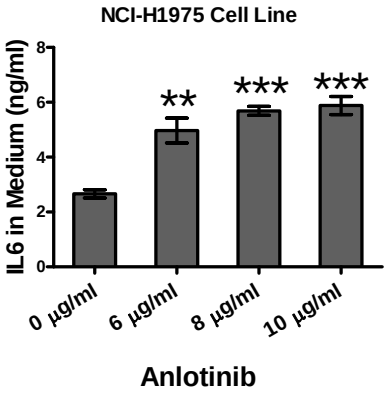

f

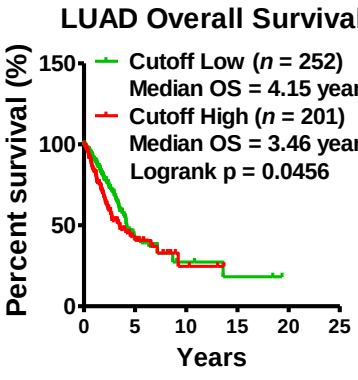

g

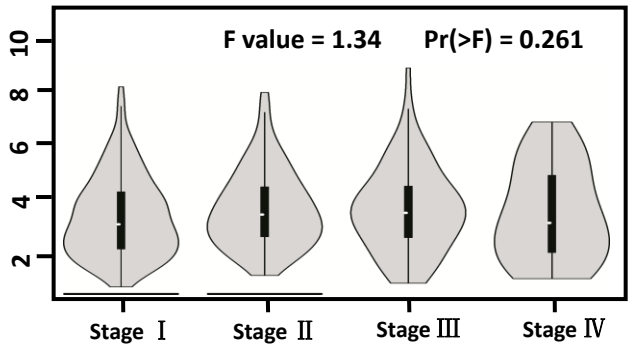

Supplementary Figure 4. Anlotinib-induced IL6 alterations are not associated with anlotinib-induced anti-angiogenesis. RNA-seq data from NSCLC patient biopsy samples (*n* = 947) and clinical data from NSCLC patients (*n* = 947) were analysed for the correlation of CCL2 expression and prognosis. (a) Kaplan-Meier plots of overall survival in NSCLC patients based on CCL2 expression stratification. Cut-off-high = 515; cut-off-low = 432. (b) CCL2 expression levels in NSCLC patients at different stages. (c) The top 10 co-expressed genes associated with CCL2 in LUAD patients. The significance of the correlation was determined using Pearson's correlation coefficient (PCC). (d) Correlation analysis of CCL2 and IL6 expression in LUAD patients. The significance of the CCL2-IL6 correlation was determined using PCC. (e) Alterations of IL6 levels after anlotinib (0 μg/ml, 6 μg/ml, 8 μg/ml and 10 μg/ml) administration in NCI-H1975 cells. Bars = mean ± SD, *n* = 3, ***P*< 0.01, ****P*< 0.001. (f) RNA-seq data from LUAD patient biopsy samples (*n* = 453) and clinical data from LUAD patients (*n* = 453) were analysed for the correlation of IL6 expression and prognosis. Cut-off-high = 201; cut-off-low = 252. (g) IL6 levels in LUAD patients at different stages.

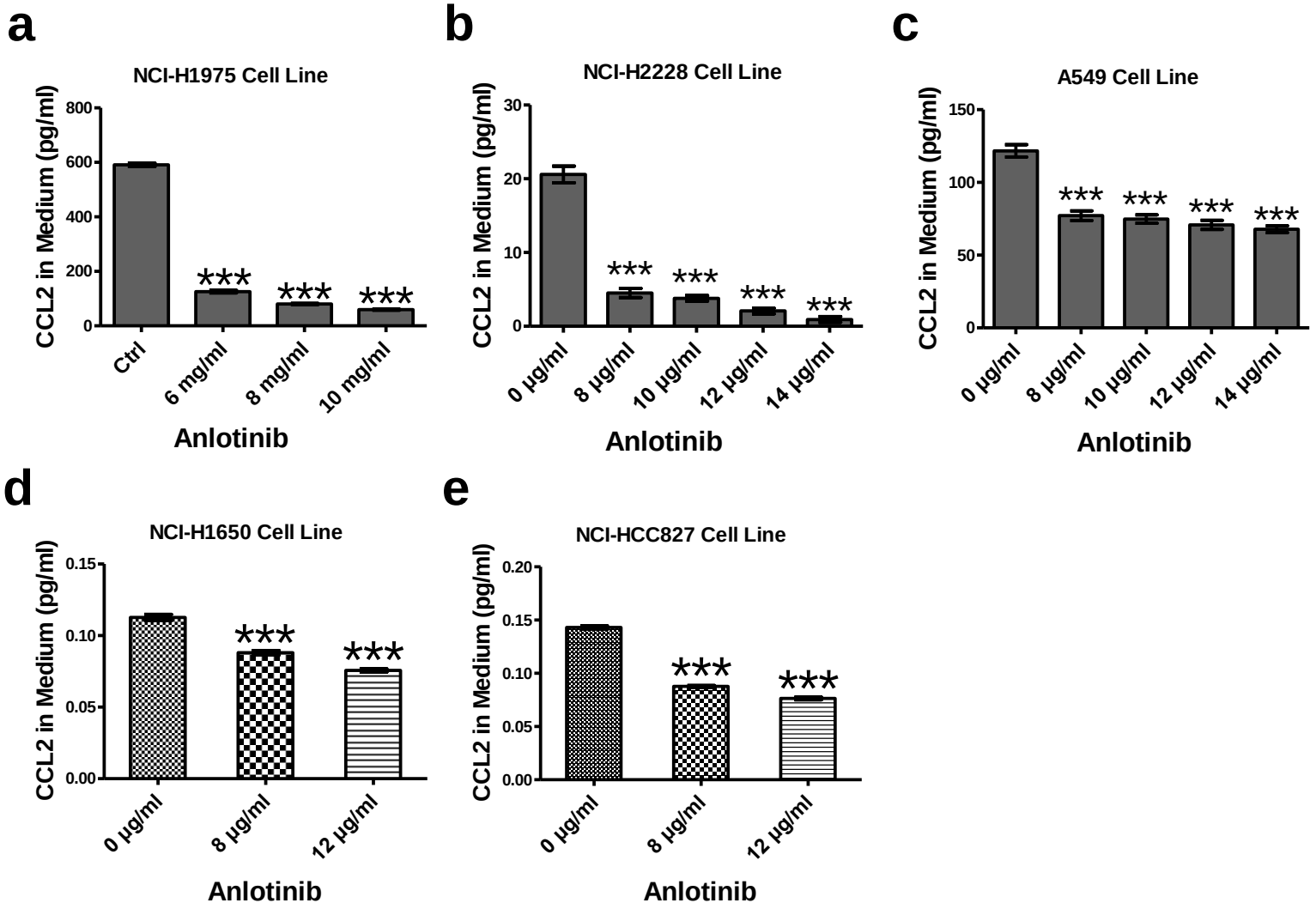

Supplementary Figure 5. Anlotinib inhibits CCL2 expression in LUAD cell lines. LUAD cell lines (including NCI-H1975 cells, NCI-H2228 cells, A549 cells, NCI-H1650 cells and NCI-HCC827 cells) were exposed to anlotinib for 24 hours, and the contents of CCL2 in medium were measured by ELISA. (a) Alteration of the medium CCL2 concentration before and after anlotinib (6 μg/ml, 8 μg/ml and 10 μg/ml) administration in NCI-H1975 cells. Bars = mean ± SD, $n = 3$, ***$P < 0.001$. (b, c) Alteration of the medium CCL2 concentration after anlotinib (0 μg/ml, 8 μg/ml, 10 μg/ml, 12 μg/ml and 14 μg/ml) administration in NCI-H2228 and A549 cells. Bars = mean ± SD, $n = 3$, ***$P < 0.001$. (d, e) Alteration of the medium CCL2 concentration after anlotinib (0 μg/ml, 8 μg/ml and 12 μg/ml) administration in NCI-H1650 and NCI-HCC827 cells. Bars = mean ± SD, $n = 3$, ***$P < 0.001$.

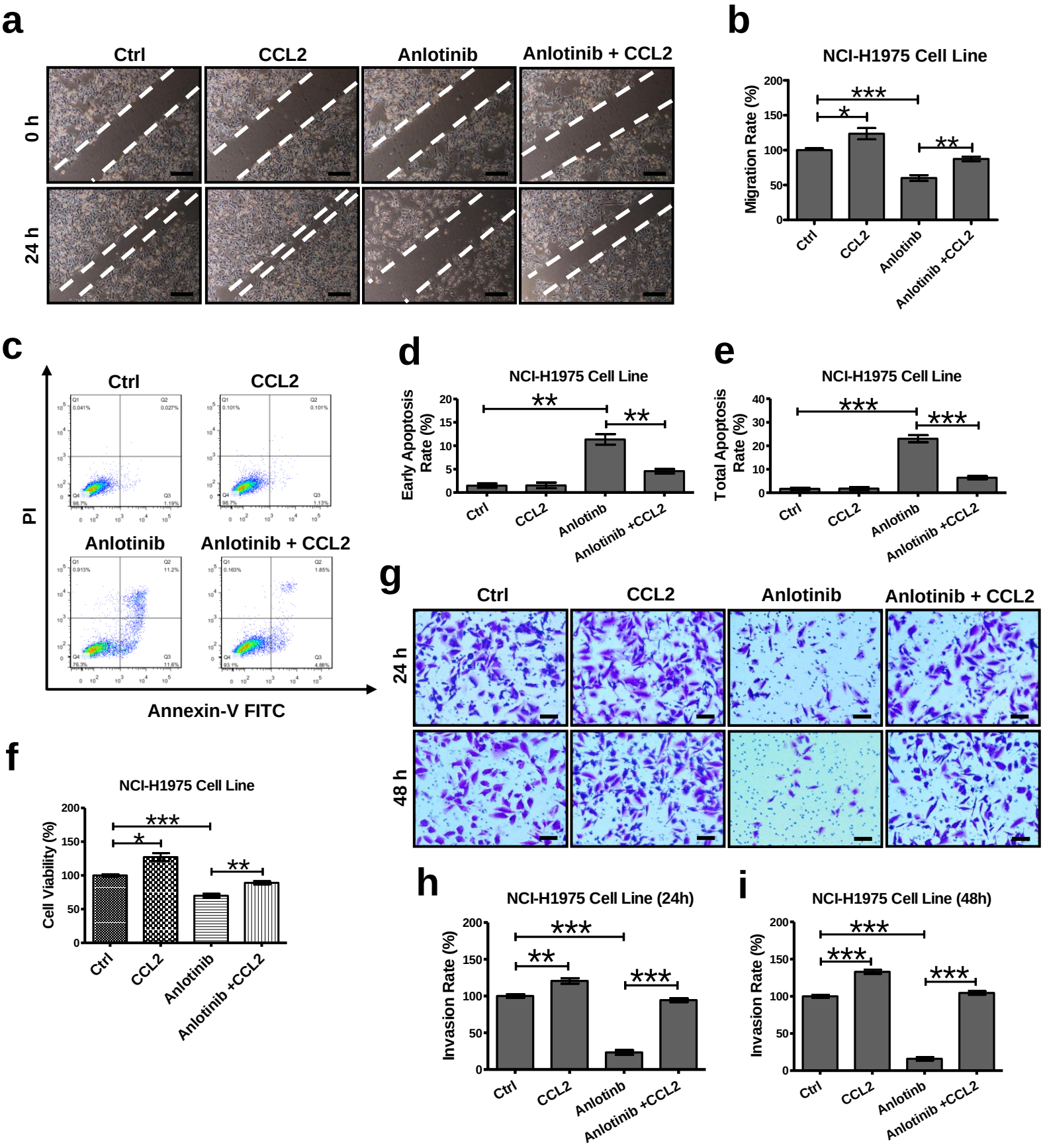
a
Ctrl
CCL2
Anlotinib
Anlotinib + CCL2
0 h
24 h
b
NCI-H1975 Cell Line
Migration Rate (%)
Ctrl
CCL2
Anlotinb
Anlotinib +CCL2
c
Ctrl
CCL2
Anlotinib
Anlotinib + CCL2
PI
Annexin-V FITC
d
NCI-H1975 Cell Line
Early Apoptosis Rate (%)
e
NCI-H1975 Cell Line
Total Apoptosis Rate (%)
f
NCI-H1975 Cell Line
Cell Viability (%)
g
Ctrl
CCL2
Anlotinib
Anlotinib + CCL2
24 h
48 h
h
NCI-H1975 Cell Line (24h)
Invasion Rate (%)
i
NCI-H1975 Cell Line (48h)
Invasion Rate (%)

Supplementary Figure 6. Replenishment of exogenous CCL2 offsets anlotinib-induced cytotoxicity in NCI-H1975 cells. (a, b) NCI-H1975 cells were exposed to CCL2 (50 ng/ml) and anlotinib (4 μg/ml), alone or together, for 24 hours. The wound-healing scratch assay was performed to evaluate the migration rate. Bars = mean ± SD, n = 3, *P< 0.05, **P< 0.01, ***P< 0.001. (c-e) NCI-H1975 cells were exposed to CCL2 (50 ng/ml) and anlotinib (4 μg/ml), alone or together, for 24 hours. The apoptotic process was detected by flow cytometry. The ratios of early apoptosis and total apoptosis were analysed based on flow cytometric detection. Bars = mean ± SD, n = 3, **P< 0.01, ***P< 0.001. (f) NCI-H1975 cells were exposed to CCL2 (50 ng/ml) and anlotinib (4 μg/ml), alone or together, for 24 hours. Cell viabilities were measured using the CCK8 kit. Bars = mean ± SD, n = 3, *P< 0.05, **P< 0.01, ***P< 0.001. (g-i) NCI-H1975 cells were exposed to CCL2 (50 ng/ml) and anlotinib (2 μg/ml), alone or together, for 24 and 48 hours, respectively. Statistical analysis of the invasion rate based on transwell assays. Bars = mean ± SD, n = 5, **P< 0.01, ***P< 0.001.

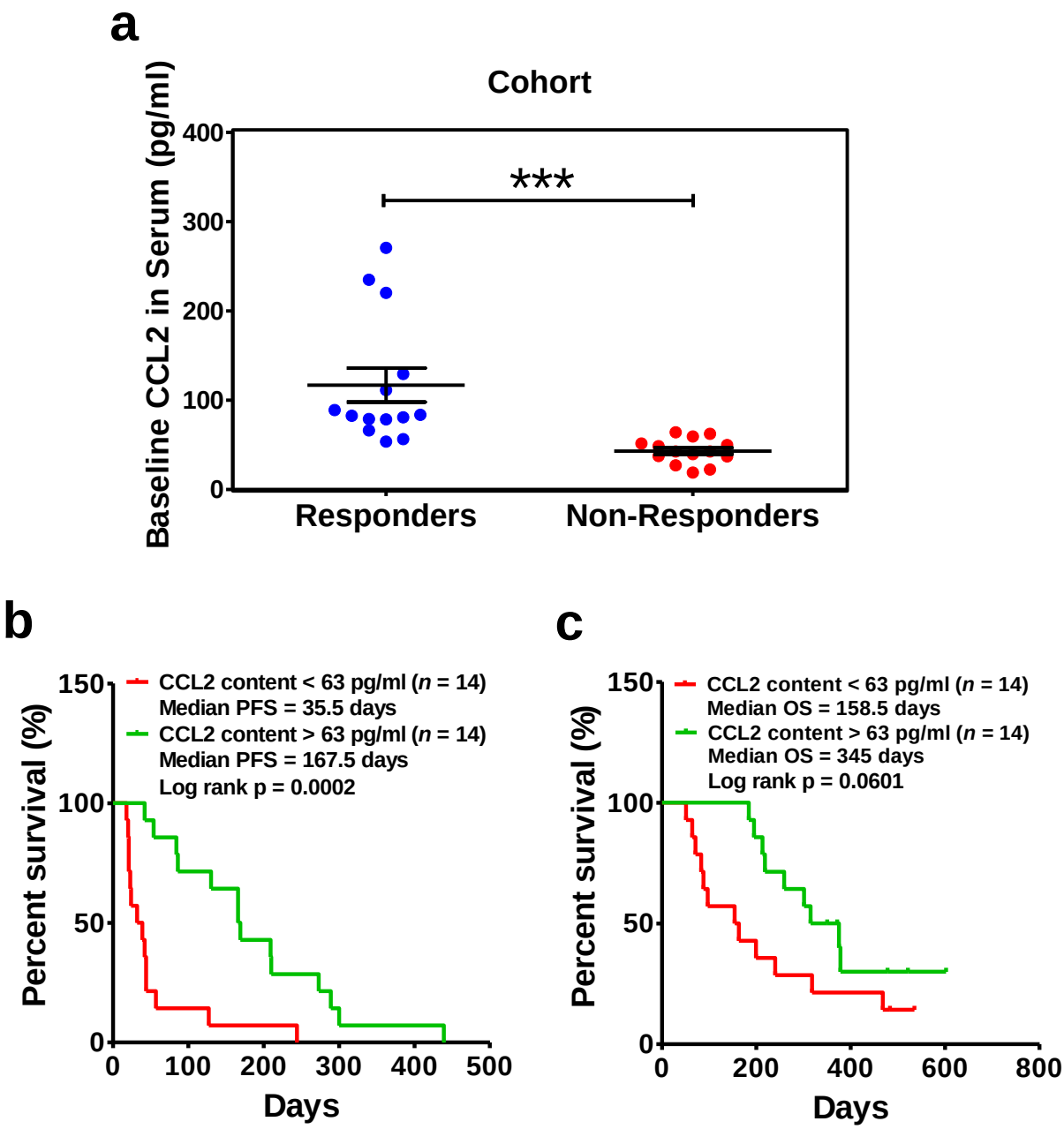

Supplementary Figure 7. Serum CCL2 levels at baseline predict the response to anlotinib in refractory advanced NSCLC patients. (a) Serum CCL2 levels at baseline in advanced refractory NSCLC patients consisted of anlotinib responders and anlotinib non-responder. Bars = mean ± SD, n = 14, ***P< 0.001. (b) Kaplan-Meier curves of PFS stratified by serum CCL2 levels in advanced refractory NSCLC patients receiving anlotinib therapy. n = 28, cut-off-high: 50%; cut-off-low: 50%,

median PFS: 35.5 days (95% CI 0-71) vs 167.5 days (95% CI 104-231), log rank *P* = 0.0002. (c) Kaplan-Meier curves of OS stratified by the serum CCL2 levels in advanced refractory NSCLC patients receiving anlotinib therapy. *n* = 28, cut-off-high: 50%; cut-off-low: 50%, median OS: 158.5 days (95% CI 61-256) vs 345 days (95% CI 272-418), log rank *P* = 0.0601.

Supplementary Methods

Patients and samples. Patients bearing refractory advanced NSCLC were registered at Shanghai Chest Hospital, Tianjin Medical University Cancer Hospital, Henan Province Tumor Hospital, Peking Union Medical College Hospital, Linyi City Tumor Hospital, Shandong Province Tumor Hospital, Jilin Province Tumor Hospital, First Affiliated Hospital of Guangzhou Medical University, Chinese Academy of Medical Sciences Cancer Hospital, Lanzhou Military General Hospital, Qilu Hospital, Hunan Province Tumor Hospital, First Affiliated Hospital of Xi'an Jiaotong University, Tangdu Hospital, Beijing Chest Hospital of Capital Medical University, Jiangxi Province Tumor Hospital, The First Affiliated Hospital of Zhejiang University and Chongqing Cancer Hospital. The patients were confirmed to have advanced NSCLC (IIIB/IV stage) and had been receiving chemotherapy or driver gene inhibitors for at least two lines of therapy.[1-3] The patients received anlotinib as third-line therapy or beyond. Each cycle of medication for these patients consisted of anlotinib (12 mg/day) for two consecutive weeks and then discontinuation for one week. All patients received multiple cycles of anlotinib therapy until disease progression or intolerable toxicity occurred. Computed tomography (CT) was performed no more than 2 weeks before anlotinib therapy. After treatment initiation, tumours were evaluated once per cycle during the first two cycles and then once every two cycles. The patients who completed the anlotinib trial were followed up every eight weeks. Blood sample collections as well as CT evaluations were also performed. All patients provided written informed consent. The trial was registered at ClinicalTrials.gov under No. NCT02388919.

Cell culture. Procedures for cell culture were performed according to our previous studies.[4, 5] Briefly, the human LUAD cell lines NCI-H1975 ($EGFR^{L858R,\ T790M}$ mutation), PC-9 ($EGFR^{L858R}$ mutation), HCC-827 ($EGFR^{\text{Exon 19 deletion}}$ mutation), A549 ($EGFR^{\text{wild type}}$), NCI-H2228 (EML4-ALK fusion) and NCI-H1650 ($EGFR^{\text{Exon 19 deletion}}$, PTEN loss) were obtained from ATCC: The Global Bioresource Center (https://www.atcc.org/). All cell lines were validated to contain no mycoplasma

contamination using the TransDetect PCR Mycoplasma Detection Kit (TransGen, China). Cells were maintained in RPMI 1640 medium (Gibco, USA) supplemented with 10% foetal bovine serum (FBS) (Gibco, USA) and 100 units/ml of penicillin and streptomycin (Gibco, USA). The cells were incubated at 37℃ in a humidified atmosphere of 5% CO_2.

Cell viability analysis. Cells were cultured at 1500 cells per well in 96-well plates for 24 hours and then treated with anlotinib for 24 hours. The cell counting kit 8 (CCK8) (Dojindo, Japan) was used to evaluate cell viability according to the manufacturer's protocol. Cell viabilities were calculated by measuring the optical density at 450 nm using a spectrophotometric plate reader (Bio-Tek, USA). The absorbance of the control sample was set at 100% viability, and the absorbance of cell-free wells containing medium was set at zero. All cell viability results were tested in three independent experiments.

Flow cytometric analysis. To analyse apoptotic cells, the Annexin V-FITC/PI Apoptosis kit (Zoman Biotechnology Co., Ltd, China) was used to determine the phosphatidyl serine content and membrane integrity of each cell. The detailed procedures were performed according to our previous studies.[4, 5] Cells were stained with Annexin V-FITC and PI simultaneously and then detected by flow cytometry (BD LSRFortessa, USA). PI-positive cells were designated as end-stage apoptotic cells, and FITC-positive cells were designated as early-stage apoptotic cells. To evaluate anlotinib-induced apoptosis, 5×10^5 NCI-H1975 cells were cultured in 6-well plates for 24 hours and then treated with anlotinib (8 μg/ml) for 24 hours. To assess whether replenishment with exogenous human recombinant CCL2 (Pepro Tech, USA) could offset anlotinib-induced apoptosis, 5×10^5 NCI-H1975 cells were cultured in 6-well plates for 24 hours and then were exposed to CCL2 (50 ng/ml) and anlotinib (6 μg/ml), alone or together, for 24 hours. To analyse the cell cycle, PI (Aladdin, China) was used to stain anlotinib-treated and non-treated cells. All prepared samples were detected by flow cytometry (BD LSRFortessa, USA). The ratios of G1-phase, G2-phase and S-phase were analysed based on flow cytometric detection.

Cell invasion. Invasion assays were performed using a transwell filter (8-μm pore size; Corning, USA). Transwell membranes were coated with Matrigel matrix (diluted with 1:8; Corning, USA). NCI-H1975 cells were starved overnight in RPMI 1640 (Gibco, USA), then were seeded onto the top precoated chamber (5×10^4 cells per well for 24 hours evaluation; 2×10^4 cells per well for 48 hours evaluation) in 100 μl of FBS-free medium. RPMI 1640 medium with 15% FBS was placed in the bottom chamber. After a 24-or 48-hour incubation at 37℃ in 5% CO_2, the lower surface of the membrane with invasive NCI-H1975 cells was fixed with 3.7% paraformaldehyde for 30 minutes, stained with 0.1% crystal violet for 2 hours, and then washed twice with PBS. Fluorescence microscopy (Nikon, Japan) was used to capture images and quantify the number of cells per field.

Wound-healing scratch assay. Wound-healing scratch assays were performed to assess the NCI-H1975 cell migration. A total of 1×10^6 cells were cultured in 6-well plates for 24 hours and starved overnight in RPMI 1640 (Gibco, USA); then, a scratch wound was created using 200-μl pipette tip. The medium was replaced with fresh RPMI 1640 medium (Gibco, USA) supplementary with 10% FBS. For evaluation anlotinib-induced migration inhibition, samples were treated with anlotinib (6 μg/ml) for 24 hours. For assessment CCL2-induced migration recovery, samples were treated with anlotinib (4 μg/ml) and human recombinant CCL2 (50 ng/ml), alone or together, for 24 hours. Images of cell migration were captured by microscopy (Nikon, Japan), and the migration rate was calculated based on the change of wound width.

Cell immunofluorescence assays. NCI-H1975 cells were cultured in a glass-bottom cell culture dish (NEST, USA) for 24 hours and then treated with anlotinib (4 μg/ml) and CCL2 (50 ng/ml), alone or together, for 24 hours. The cell culture dishes were washed two times with PBS, fixed with 4% PFA for 30 minutes, and blocked with blocking buffer (5% goat serum and 0.3% Triton-100) for 1 hour. Primary antibodies against MMP9 (1:200, Abcam, USA), CD31 (1:200, BD/PMG, USA) and Ki67 (1:200, Abcam, USA) were incubated to bind specific proteins, followed by anti-rabbit Alexa Fluor®647-conjugated (1:1000, CST, USA) and anti-mouse Alexa

Fluor®488-conjugated (1:1000, CST, USA) secondary antibodies. Finally, all samples were stained with Hoechst33324 for nuclear observation. Fluorescently labelled cells were observed using confocal laser scanning microscopy (CLSM) (Nikon, Japan).

Animal experiments. Experiments using Balb/c nude mice (SLAC Laboratory Animal) were performed according to national guidelines for welfare. All of the mice used in the present study were female and aged 4-6 weeks. All mice had free access to food and water throughout the experimental period. To induce the NCI-H1975-derived xenograft model, 5×10^6 NCI-H1975 cells in Reduced Matrigel® Matrix Growth Factor (Corning, USA) were subcutaneously injected in the right fore-lateral abdomen.

To assess the anti-tumour effect of anlotinib, the mice were divided into three groups: Ctrl, anlotinib 1 and anlotinib 2. The anlotinib treatments (anlotinib 1, 1.5 mg/kg and anlotinib 2, 2.25 mg/kg) were administered 14 days after NCI-H1975 cell injection via gavage for two consecutive weeks and then discontinued for one week. Saline was administered in the Ctrl group. To evaluate whether the replenishment of exogenous CCL2 could recover anlotinib-induced anti-angiogenesis *in vivo*, the mice were divided into three groups: Ctrl, anlotinib and anlotinib + CCL2. Anlotinib (2.5 mg/kg) treatment was described above. CCL2 (R&D systems, USA; 5 μg/kg, iv, qod) treatment was performed via tail intravenous injection.

Body weight and tumour volume were measured three times per week. Tumour volume was calculated based on the following formula: volume = length × width^2/2. The fold change in tumour growth was calculated based on the following formula: fold change = tumour volume of Day n/ tumour volume of Day 1. Serum was collected on Day 5 and Day10. When the tumour volume of any mouse reached the maximal value allowed under our institutional protocol, serum collection and tumour tissue collection were performed immediately for all mice. Tumours were collected and weighed. All serum samples were stored at -80 ℃. Half of the tumour samples from each mouse were fixed using 4% PFA, and the other half were stored at -80 ℃.

Histology analysis. Tumour tissue was stored at -80℃ (Thermo, USA) and then sectioned at a thickness of 8-10 μm using a freezing microtome (Leica, Germany). For general observations, sections on glass slides were dehydrated and then stained with haematoxylin and eosin (H&E). For immunofluorescent histochemical observation, the sections on glass slides were incubated with primary antibody against CD31 (1:50, BD/PMG, USA),Ki67 (1:200, Abcam, USA) or MMP9 (1:100, Abcam, USA) and then with Alexa Fluor®647-conjugated secondary antibody. For vessel staining, lectin (1:100, VECTOR, USA) was incubated with the samples for 24 hours. Finally, the slides were stained with Hoechst33324 for nuclear observations. All fluorescently labelled slides were observed using confocal laser scanning microscopy (CLSM) (Nikon, Japan).

RNA-seq library. NCI-H1975 cells were cultured in 6-well plates for 24 hours and then treated with anlotinib (8 μg/ml) for 24 hours. TRIzol reagent (Life Technologies, Inc., USA) was used to lyse cell samples, followed by total RNA isolation using standard procedures. mRNA was isolated using the Oligotex mRNA Mini Kit (Qiagen, Germany). Residual genomic DNA was degraded by adding DNase (NEB, USA), followed by incubation for 30 minutes at 37℃. Next, 100 ng mRNA from each sample was reverse-transcribed into cDNA and fragmented into 100-300-bp pieces. The NEBNext Ultra Directional RNA Library Prep Kit (NEB, USA) was used to end-repair and adapter-ligate the fragmented cDNA. The samples were amplified using 10 cycles in a thermal cycler in PCR Master Mix supplemented with Q5 High-Fidelity DNA Polymerase (NEB, USA). The PCR products were quantified using an Agilent 2100 bioanalyzer (Agilent, USA), and standard paired-end sequencing with 75-bp reads was performed using the Illumina Next500 (Illumina, USA) sequencing platform. The raw data for this study are available in the EMBL database under accession number E-MTAB-5997: http://www.ebi.ac.uk/arrayexpress/.

Analysis of RNA-seq raw data. The raw sequencing reads were extracted and analysed using Illumina software. The sequencing quality was detected using FastQC software. All qualified sequence tags were mapped to the reference genome (hg38) by

TopHat.[6] Cufflinks was used to characterize the differential transcription pattern. Biases in library preparation were taken into account. The gene expression level was measured by the reads per kilo-base of transcript per million mapped reads (FPKM). To analyse the gene expression difference between anlotinib-treated samples and the Ctrl sample, we selected genes with an expression level exhibiting at least a two-fold change. According to the analytical method, a $\log2^{\text{Fold Change}} > 1$ represented a gene expression level that was least two-fold up-regulated, and a $\log2^{\text{Fold Change}} < -1$ represented a gene expression level that was at least two-fold down-regulated.

Functional annotation, pathway analysis and Panther analysis. Analyses of gene function clusters and pathway clusters were performed using a public bioinformatics resource platform named Database for Annotation, Visualization and Integrated Discovery (DAVID, https://david.ncifcrf.gov/).[7] Briefly, a list of differentially expressed genes was uploaded to DAVID Bioinformatics Resources 6.7, and gene ontology (GO) cluster and Kyoto Encyclopaedia of Genes and Genomes (KEGG) pathway cluster analyses were performed. Panther analysis was also performed using the Panther Classification System (http://www.pantherdb.org/).

mRNA expression analysis. NCI-H1975 cells were cultured in 6-well plates for 24 hours and then treated with anlotinib (8 μg/ml) for 24 hours. Total RNA isolation was performed as previously mentioned. RNA was purified using the RNeasy kit (Qiagen, Germany) according to the manufacturer's protocol. Reverse transcription was performed using random primers and SuperScrip®IIIReverse Transcriptase (Invitrogen, USA). RT-qPCR was performed to analyse target gene expression using SYBR Green PCR Mix (Thermo, USA). GAPDH was used as a reference control for normalization. The obtained values were expressed as n-fold changes in regulation compared with the control by applying the $2^{-\Delta\Delta Ct}$ method of relative quantification. The primer sequences used in the present study for RT-qPCR detection were as follows: *CCL2:* forward 5'-3' CAGCCAGATGCAATCAATGCC, reverse 5'-3' TGGAATCCTGAACCCACTTCT; *IL6:* forward 5'-3' AGACAGCCACTCACCTCTTC, reverse 5'-3' AGTGCCTCTTTGCTGCTTTC;

PECAM1(CD31): forward 5'-3' CCTTCAACAGAGCCAACCAC, reverse 5'-3' GGCCGCAATGATCAAGAGAG; *MKI67 (Ki67):* forward 5'-3' CACGAGACGCCTGGTTACTA, reverse 5'-3' TGACACAACAGGAAGCTGGA; *MMP-1:* forward 5'-3' TCATGCTTTTCAACCAGGCC, reverse 5'-3' TCATGAGCTGCAACACGATG; *MMP-2:* forward 5'-3' TGCTCCACCACCTACAACTT, reverse 5'-3' GCAGCTGTCATAGGATGTGC;*MMP-3:* forward 5'-3' CCTGGAAATGTTTTGGCCCA, reverse 5'-3' GGCTGAGTGAAAGAGACCCA; *MMP-9:* forward 5'-3' TGCCACTTCCCCTTCATCTT, reverse 5'-3' CGTCCTGGGTGTAGAGTCTC; *MMP-19:* forward 5'-3' ACTTCCAGTCTCAGGTCAGC, reverse 5'-3' GCAGGTTCAAGATGCGGAAA; and GAPDH: forward 5'-3' AGGTCGGAGTCAACGGATTT, reverse 5'-3' TGACAAGCTTCCCGTTCTCA.

ELISA. All ELISA kits for CCL2 and IL6 detection were purchased from eBioscience. For the *in vitro* experiments, the culture media of NCI-H1975, NCI-H2228, A549, NCI-H1650 and NCI-HCC827 cells were collected after anlotinib treatment. For the *in vivo* experiments, serum was obtained at different time points after anlotinib administration. The tumour tissue homogenate was collected at the end of the animal experiment. CCL2 levels were evaluated using mCCL2 Platinum ELISA (eBioscience, USA) for mice and hCCL2 Platinum ELISA (eBioscience, USA) for humans. IL-6 levels were assessed using hIL6 Platinum ELISA (eBioscience, USA). All experimental procedures were performed according to the manufacturer's protocol.

Analysis of the TCGA cohort. RNA-seq data and clinical data for NSCLC (including LUAD and LUSC) were downloaded from the TCGA data portal (https://cancergenome.nih.gov/). In total, 453 clinical data and RNA-seq data accounted for LUAD, and 494 clinical data and RNA-seq data accounted for LUSC. All data were parsed using a custom R function. The FPKM expression values were transformed to log2 counts per million using the voom function from the limma R

package. Cut-off values for CCL2 and IL6 were defined using the "Ward method". Co-expression analysis of CCL2 and correlation analysis of CCL2-IL6 were performed according to the Gene Expression Profiling Interactive Analysis (GEPIA) (http://gepia.cancer-pku.cn/index.htmL).

References

1. Han BH, Li K, Wang QM, et al. Effect of Anlotinib as a Third-Line or Further Treatment on Overall Survival of Patients With Advanced Non–Small Cell Lung Cancer The ALTER 0303 Phase 3 Randomized Clinical Trial. JAMA Oncol. 2018; doi:10.1001/jamaoncol.2018.3039.
2. Han BH, Li K, Zhao YZ, et al. Anlotinib as a third-line therapy in patients with refractory advanced non-small-cell lung cancer: a multicentre, randomised phase II trial (ALTER0302). Br J Cancer. 2018; doi: 10.1038/bjc.2017.478.
3. Han BH, Li K, Wang QM, et al. Efficacy and safety of third-line treatment with anlotinib in patients with refractory advanced non-small-cell lung cancer (ALTER-0303): a randomised, double-blind, placebo-controlled phase 3 study. Lancet Oncol. 2017; 18: S3-S3.
4. Zhang XL, Wu J, Wang J, et al. Integrative epigenomic analysis reveals unique epigenetic signatures involved in unipotency of mouse female germline stem cells. Genome Biol. 2016; 17(1): 162.
5. Lu J, Chen J, Xu N, et al. Activation of AIFM2 enhances apoptosis of human lung cancer cells undergoing toxicological stress. Toxicol Lett. 2016; 258: 227-36.
6. Trapnell C, Roberts A, Goff L, et al. Differential gene and transcript expression analysis of RNA-seq experiments with TopHat and Cufflinks. Nat Protoc. 2012; 7(3): 562-78.
7. Huang DW, Sherman BT, Tan Q, et al. DAVID Bioinformatics Resources: expanded annotation database and novel algorithms to better extract biology from large gene lists. Nucleic Acids Res. 2007; 35: W169-75.